

1 **Photoelectro-Fenton treatment of pesticide triclopyr at neutral pH**  
2 **using Fe(III)-EDDS under UVA light or sunlight**

3 Izabelle C. Da Costa Soares<sup>1,2</sup>, Roger Oriol<sup>1#</sup>, Zhihong Ye<sup>1,3#</sup>, Carlos A.  
4 Martínez-Huitle<sup>2</sup>, Pere L. Cabot<sup>1</sup>, Enric Brillas<sup>1</sup>, Ignasi Sirés<sup>1\*</sup>

5 <sup>1</sup> *Laboratori d'Electroquímica dels Materials i del Medi Ambient, Departament de Química*  
6 *Física, Facultat de Química, Universitat de Barcelona, Martí i Franquès 1-11, 08028*  
7 *Barcelona, Spain*

8 <sup>2</sup> *Laboratório de Eletroquímica Ambiental e Aplicada, Instituto de Química, Universidade*  
9 *Federal do Rio Grande do Norte, Lagoa Nova - CEP 59.072-900, Natal, RN, Brazil*

10 <sup>3</sup> *Environmental Engineering Research Centre, Department of Civil Engineering, The*  
11 *University of Hong Kong, Pokfulam, Hong Kong, China*

12  
13  
14  
15  
16  
17  
18  
19  
20  
21 \*Corresponding author: E-mail address: i.sires@ub.edu (Ignasi Sirés)

22 # Both authors contributed equally to this work.

23

24 **Abstract** One of the main challenges of electrochemical Fenton-based processes is the  
25 treatment of organic pollutants at near-neutral pH. As a potential approach to this problem, this  
26 work addresses the use of a low content of soluble chelated metal catalyst, formed between  
27 Fe(III) and ethylenediamine-*N,N'*-disuccinic (EDDS) acid (1:1), to degrade the herbicide  
28 triclopyr in 0.050 M Na<sub>2</sub>SO<sub>4</sub> solutions at pH 7.0 by photoelectro-Fenton with UVA light or  
29 sunlight (PEF and SPEF, respectively). Comparison with electro-Fenton treatments revealed  
30 the crucial role of the photo-Fenton-like reaction, since this promoted the production of soluble  
31 Fe(II) that enhanced the pesticide removal. Hydroxyl radicals formed at the anode surface and  
32 in the bulk were the main oxidants. A boron-doped diamond (BDD) anode yielded a greater  
33 mineralization than an IrO<sub>2</sub>-based one, at the expense of reduced cost-effectiveness. The effect  
34 of catalyst concentration and current density on the performance of PEF with BDD was  
35 examined. The PEF trials in 0.25 mM Na<sub>2</sub>SO<sub>4</sub> + 0.35 mM NaCl medium showed a large  
36 influence of generated active chlorine as oxidant, being IrO<sub>2</sub> more suitable than RuO<sub>2</sub> and BDD.  
37 In SPEF with BDD, the higher light intensity from solar photons accelerated the removal of the  
38 catalyst and triclopyr, with small effect on mineralization. A plausible route for the herbicide  
39 degradation by Fe(III)–EDDS-catalyzed PEF and SPEF is finally proposed based on detected  
40 byproducts: three heteroaromatic and four linear *N*-aliphatic compounds, formamide and  
41 tartronic and oxamic acids.

42 *Keywords:* Ethylenediamine-*N,N'*-disuccinic (EDDS) acid; Hydroxyl radical; Pesticide;  
43 Photoelectro-Fenton; Sunlight; Triclopyr; Water treatment

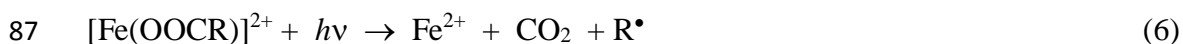
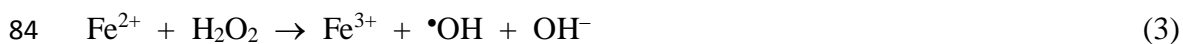
## 44 **Introduction**

45 In recent years, the treatment of biorecalcitrant organic pollutants dissolved in water by  
46 electrochemical advanced oxidation processes (EAOPs) such as electrochemical oxidation  
47 (EO), electro-Fenton (EF) and photoelectro-Fenton (PEF) has received substantial attention  
48 (Brillas and Martínez-Huitle 2015; Ganiyu et al. 2018; Martínez-Huitle and Panizza 2018). PEF  
49 is the most complex process, since it combines the oxidation ability of EO and EF with the  
50 photolytic action of UVA photons (Martínez-Huitle et al. 2015). Artificial UVA light can be  
51 replaced by natural sunlight to increase the sustainability of the technology, giving rise to the  
52 so-called solar PEF (SPEF) process (Brillas 2014; Pérez et al. 2017). The common feature of  
53 EF, PEF and SPEF processes is the continuous electrochemical generation of Fenton's reagent  
54 ( $\text{Fe}^{2+}$  plus  $\text{H}_2\text{O}_2$ ), a mixture that ensures the in-situ production of hydroxyl radical ( $\bullet\text{OH}$ ) in the  
55 bulk. This strong oxidant can react non-selectively and very quickly with most organics thanks  
56 to its high standard reduction potential ( $E^\circ$ ) of 2.73 V/SHE. Usually, pure  $\text{O}_2$  or air is pumped  
57 into the system to allow the reduction reaction (1) at a suitable carbonaceous cathode. Carbon  
58 felt is a cheap cathode to do this (El-Ghenymy et al. 2014; Ganzenko et al. 2018), but air-  
59 diffusion cathodes may be preferred because of the larger  $\text{H}_2\text{O}_2$  production (Galia et al. 2016;  
60 El-Ghenymy et al. 2015; Roth et al. 2016; Lanzalaco et al. 2017; Ye et al. 2019b).



62 The application of EO process, which requires relatively simple setups, induces the  
63 destruction of organics by adsorbed hydroxyl radical ( $\text{M}(\bullet\text{OH})$ ) that is formed as  $\text{O}_2$  evolves  
64 during water oxidation at the anode M, as represented in reaction (2) (Martínez-Huitle et al.  
65 2015). Non-active anodes like boron-doped diamond (BDD) are optimum to generate very  
66 reactive and oxidizing ( $\text{M}(\bullet\text{OH})$ ) because of their higher  $\text{O}_2$ -evolution overpotential as  
67 compared to active anode materials like Pt and dimensionally stable anodes (DSA) (Steter et

68 al. 2016; Clematis et al. 2017; Lanzalaco et al. 2018; Ridruejo et al. 2018). When EO is  
 69 performed in a one-compartment cell and the cathode produces H<sub>2</sub>O<sub>2</sub> via reaction (1), it is so-  
 70 called EO with electrogenerated H<sub>2</sub>O<sub>2</sub> (EO-H<sub>2</sub>O<sub>2</sub>). The mild oxidation caused by H<sub>2</sub>O<sub>2</sub> becomes  
 71 powerful in the presence of dissolved Fe<sup>2+</sup>, originating the EF process, in which the oxidant  
 72 •OH is formed in the bulk from Fenton's reaction (3) at optimum pH ~ 3.0 (Vasudevan and  
 73 Oturan 2014; Ganiyu et al. 2018). Although the electroreduction of Fe<sup>3+</sup> to Fe<sup>2+</sup> via reaction (4)  
 74 is feasible at some cathodes (Yahya et al. 2014; Yang et al. 2019), the regeneration of ferrous  
 75 ion is more effective using UVA radiation (λ = 320-400 nm) in PEF or sunlight (λ > 300 nm)  
 76 in SPEF. In such systems, the UV photons cause the photolysis of hydrated Fe(III) species,  
 77 which are photoactive at pH near 3.0, via photo-Fenton reaction (5), having a positive impact  
 78 on the rate of destruction of the target pollutant (Brillas 2014; Pérez et al. 2017). In addition,  
 79 the formation of short-linear carboxylic acids upgrades the mineralization degree because their  
 80 Fe(III) complexes are photodecomposed via reaction (6) (Brillas 2014; Martínez-Huitle et al.  
 81 2015). In the PEF and SPEF processes, the anode composition usually has low significance due  
 82 to the predominant role of photoreduction reactions.



88 EF, PEF and SPEF are very efficient to degrade the organic matter under acidic solutions.  
 89 However, the progressive precipitation of Fe(OH)<sub>3</sub> as pH increases is highly detrimental and  
 90 hence, these processes are considered quite inefficient at circumneutral pH. Accordingly,  
 91 unconventional approaches have been developed, including heterogeneous Fenton treatments

92 with solid iron catalysts (Ye et al. 2020b) and homogeneous processes with soluble chelated  
 93 iron (Clarizia et al. 2017; Ganiyu et al. 2018). In previous work, some of us explored the  
 94 viability of chelators like oxalate for pentachlorophenol degradation by solar photo-Fenton (Ye  
 95 et al. 2019c) and ethylenediamine-*N,N'*-disuccinic acid (EDDS) to destroy butylated  
 96 hydroxyanisole by EF (Ye et al. 2019a) and fluoxetine by PEF (Ye et al. 2020a). EDDS has  
 97 been found more interesting because of its biodegradability and the high efficiency of Fe(III)–  
 98 EDDS-catalyzed treatments at neutral pH (Miralles-Cuevas et al. 2019). Fe(III)–EDDS can be  
 99 reduced via the Fenton-like reaction (7) and then, the produced Fe(II)–EDDS catalyzes the  
 100 H<sub>2</sub>O<sub>2</sub> decomposition to •OH via reaction (8) (Zhang et al. 2016), which predominates over  
 101 Fenton's reaction (3) at neutral pH. The •OH production is stimulated as Fe<sup>2+</sup> is formed under  
 102 UV light irradiation, via photo-Fenton-like reaction (9), whose quantum yield is much higher  
 103 than that of classical photo-Fenton reaction (5) (Ye et al. 2020a). Note that the Fe(III)–EDDS-  
 104 catalyzed EAOPs at neutral pH reported so far have mainly addressed the treatment of aromatic  
 105 pollutants. Conversely, scarce information is available on the performance regarding the  
 106 removal of heteroaromatic contaminants, which are very abundant in natural water and urban  
 107 wastewater.



111 Triclopyr (C<sub>7</sub>H<sub>4</sub>Cl<sub>3</sub>NO<sub>3</sub>, 3,5,6-trichloro-2-pyridyloxyacetic acid, *M* = 256,46 g mol<sup>-1</sup>) is a  
 112 selective pyridine herbicide widely employed for controlling herbaceous plants. It presents low  
 113 toxicity in mammals, like rats and rabbits, and birds, but it has been found moderately toxic to  
 114 sensitive aquatic biota like fish and larval amphibians (Edginton et al. 2003; Senseman 2007;  
 115 Li et al. 2018). Triclopyr has been detected in soil and surface water at concentrations up to 3

116  $\mu\text{g L}^{-1}$  in different countries like USA (Battaglin et al. 2009) and Australia (Rippy et al. 2017).  
117 Despite being recalcitrant to photodegradation and oxidation, this pesticide has been efficiently  
118 degraded by several photo-assisted AOPs like photocatalysis with  $\text{TiO}_2/\text{UV}$  (Qamar et al. 2006)  
119 and  $\text{ZnO}/\text{SnO}_2$  (Yadav et al. 2019), photocatalytic ozonation with  $\text{Au}/\text{TiO}_2$  (Maddila et al. 2015;  
120 Solís et al. 2016) and photo-assisted peroxonation (Pérez-Lucas et al. 2020). The herbicide  
121 yields 3,5,6-trichloro-2-pyridinol as primary intermediate (Janíková-Bandžuchová et al. 2015),  
122 further being converted into acetic acid (Qamar et al. 2006) or oxalic acid (Lei et al. 2018). It  
123 is of note that the treatment of triclopyr by Fenton-based EAOPs has never been reported. The  
124 development of these processes in the presence of a quite unexplored chelated iron catalyst like  
125  $\text{Fe(III)-EDDS}$  is necessary for the remediation of natural water and urban wastewater  
126 contaminated with this pesticide at neutral pH. This system has a potentially greater viability  
127 as compared to conventional Fenton-based treatments that need acidification for optimum  
128 operation.

129 This work reports the removal of the heteroaromatic herbicide triclopyr at neutral pH by  
130  $\text{EO-H}_2\text{O}_2$ , EF, PEF and SPEF, using  $\text{Fe(III)-EDDS}$  as soluble chelated iron catalyst in the three  
131 latter methods and an air-diffusion cathode in all cases. Comparative treatments were made  
132 with an  $\text{IrO}_2$ -based or BDD anode in sulfate medium, considering the  $\text{Fe(III)-EDDS}$   
133 concentration and current density ( $j$ ) in PEF. Selected tests were carried out in a mixed sulfate  
134 + chloride medium to clarify the role of generated active chlorine. In this matrix, the  
135 performance of SPEF was analyzed with a BDD anode. Primary and final byproducts of  
136 triclopyr, the pollutant under study, were detected by high-performance liquid chromatography  
137 (HPLC) and gas chromatography-mass spectrometry (GC-MS). The study has been made with  
138 0.12 mM triclopyr, a content much higher than that found in soils and surface water, aiming to  
139 assess its mineralization process and better detect the generated products.

140

## 141 **Materials and methods**

### 142 Chemicals

143 Triclopyr (98% purity), EDDS trisodium salt solution (~ 35% in H<sub>2</sub>O) and analytical grade  
144 Fe(ClO<sub>4</sub>)<sub>3</sub> were purchased from Sigma-Aldrich. Na<sub>2</sub>SO<sub>4</sub> (99.9% purity) was purchased from  
145 Merck. Analytical grade H<sub>2</sub>SO<sub>4</sub>, NaCl and NaOH were supplied by Panreac. An acidic solution  
146 of Ti(IV) oxysulfate (Panreac) was used for H<sub>2</sub>O<sub>2</sub> determination. L-ascorbic acid (99% purity)  
147 and 1,10-phenanthroline monohydrate (99% purity) employed for the analysis of soluble iron  
148 were purchased from Sigma-Aldrich and Alfa-Aesar, respectively. Active chlorine was  
149 determined by reaction with *N,N*-diethyl-*p*-phenylenediamine (1:1) oxalate (99% purity)  
150 provided by Acros Organics. Organic solvents of HPLC or analytical grade and other chemicals  
151 used, including analytical standards of carboxylic acids, were supplied by Panreac. Ultrapure  
152 Milli-Q water (> 18.2 MΩ cm) was employed for the preparation of synthetic and analytical  
153 solutions. The combination of Fe(ClO<sub>4</sub>)<sub>3</sub> and EDDS, both at a concentration of 0.03, 0.06 or  
154 0.09 mM, gave rise to the corresponding Fe(III)–EDDS (1:1) complexes in solution, following  
155 the methodology described in earlier work (Ye et al. 2019a).

### 156 Electrolytic cells

157 Experiments were performed in an open glass tank reactor, with the same solution in  
158 contact with the anode and a cathode. In all assays, 150 mL of solution thermostated at 35 °C  
159 thanks to external water recirculated through a glass jacket and a water bath were vigorously  
160 stirred with a PTFE bar magnet at 800 rpm. Three anodes were tested: (i) an IrO<sub>2</sub>-coated Ti  
161 plate (DSA-O<sub>2</sub>) supplied by NMT Electrodes, (ii) a RuO<sub>2</sub>-coated Ti plate (DSA-Cl<sub>2</sub>) supplied  
162 by NMT Electrodes and (iii) a BDD thin-film deposited onto Si supplied by NeoCoat. The  
163 anode, with a geometric area of 3 cm<sup>2</sup>, was connected to a 3 cm<sup>2</sup> carbon-PTFE air-diffusion  
164 cathode supplied by Sainergy Fuel Cell. This cathode was fitted into a polypropylene tube, used

165 as holder and air chamber, and fed with compressed air at a flow rate of 0.9 L min<sup>-1</sup> to  
166 electrosynthesize H<sub>2</sub>O<sub>2</sub>. The electrodes were separated by a distance of about 1.0 cm.  
167 Galvanostatic experiments (i.e., at constant  $j$ ) were made with a PAR 273A potentiostat-  
168 galvanostat. The instantaneous cell voltage was monitored with a Demestres 601BR digital  
169 multimeter. The EO-H<sub>2</sub>O<sub>2</sub> and EF trials were run in the dark, whereas the PEF treatments started  
170 as a GSC TL2001 T5 6 W fluorescent black light tube lamp ( $\lambda_{\text{max}} = 360$  nm) was switched on.  
171 This lamp was placed at about 5 cm over the solution surface, yielding an irradiance of 5 W  
172 m<sup>-2</sup>. In SPEF, a mirror was placed under the cell to reflect the sunrays back into the solution as  
173 much as possible. These tests were made in sunny and clear days of 2019 summer, with an  
174 average solar UV irradiance of 28–30 W m<sup>-2</sup>.

#### 175 Apparatus and analytical methods

176 The solution pH was measured with a Crison GLP 22 pH-meter. Samples collected at  
177 selected treatment times were microfiltered (0.45  $\mu\text{m}$ ) before analysis. The determination of  
178 H<sub>2</sub>O<sub>2</sub> concentration by the titanate colorimetric method was made with a Shimadzu 1800  
179 UV/Vis spectrophotometer at  $\lambda = 408$  nm and 25 °C. The spectrophotometric procedure  
180 followed to obtain total dissolved Fe concentration has been reported elsewhere (Ye et al.  
181 2019a). Active chlorine content was determined by the *N,N*-diethyl-*p*-phenylenediamine  
182 colorimetric method using the same spectrophotometer, at  $\lambda = 515$  nm (APHA, AWWA, WEF  
183 2005).

184 The systems and procedures needed to quantify the total organic carbon (TOC) by catalytic  
185 combustion, triclopyr and Fe(III)–EDDS concentrations by reversed-phase HPLC, carboxylic  
186 acids content by ion-exclusion HPLC, and the amounts of different ions by ion chromatography  
187 (Cl<sup>-</sup>, ClO<sub>3</sub><sup>-</sup>, ClO<sub>4</sub><sup>-</sup> and NO<sub>3</sub><sup>-</sup>) and colorimetric methods (NH<sub>4</sub><sup>+</sup>), have been detailed in earlier  
188 works (Thiam et al. 2015; Steter et al. 2016). For the determination of triclopyr concentration,



189 an acetonitrile volume equal to that of the sample was added to immediately stop the  
190 degradation process. A 60:40 (v/v) acetonitrile: water (10 mM KH<sub>2</sub>PO<sub>4</sub>, pH 3.0) mixture  
191 recirculated as mobile phase at 1.0 mL min<sup>-1</sup> allow obtaining a well-defined peak at a retention  
192 time (*t<sub>r</sub>*) of 6.0 min. The identification was made at  $\lambda = 232.3$  nm, revealing limits of detection  
193 (LOD) and quantification (LOQ) of  $3.9 \times 10^{-2}$  and  $7.8 \times 10^{-2}$  mg L<sup>-1</sup>, respectively.

194 Duplicate assays were made under each experimental condition and average values are  
195 reported in this work. Figures show the error bar for each data, with 95% confidence interval.

196 The specific energy consumption per unit TOC mass (EC<sub>TOC</sub>, in kWh (g TOC)<sup>-1</sup>) was  
197 calculated in each experiment considering the TOC destroyed ( $\Delta$ TOC, in mg L<sup>-1</sup>) upon supply  
198 of a current *I* (in A) over a time *t* (in h), as shown in Eq. (10) (Steter et al., 2016):

$$199 \quad EC_{TOC} = \frac{E_{cell} I t}{V (\Delta TOC)} \quad (10)$$

200 where  $E_{cell}$  is the average cell voltage (in V) and *V* is the solution volume (in L). When *I* was  
201 varied during the trial, the final EC<sub>TOC</sub> was obtained as the sum of the partial values.

202 The byproducts accumulated after 40 min of PEF treatment of 0.12 mM triclopyr solutions  
203 containing 0.05 M Na<sub>2</sub>SO<sub>4</sub> and 0.06 mM Fe(III)–EDDS (1:1) complex, at pH 7.0 and *j* = 16.7  
204 mA cm<sup>-2</sup>, were identified by GC-MS following the procedure described elsewhere (Ye et al.  
205 2019a) and comparing the spectra with those of the NIST05 MS database. The organic  
206 compounds were separated using either a nonpolar Teknokroma Sapiens-X5ms or a polar HP  
207 INNOWAX column, both of 0.25  $\mu$ m, 30 m  $\times$  0.25 mm.

## 208 **Results and discussion**

### 209 Fe(III)–EDDS-catalyzed PEF treatment in sulfate medium

210 Before starting with the application of the different EAOPs to triclopyr degradation, the  
211 stability of the Fe(III)–EDDS complex was assessed under PEF conditions. This study was

212 carried out with 150 mL of solutions containing 0.06 mM Fe(III)–EDDS (at molar ratio of 1:1)  
213 and 0.050 M Na<sub>2</sub>SO<sub>4</sub> at pH 7.0 and 35 °C, using an IrO<sub>2</sub>-based or BDD anode and applying a  $j$   
214 = 16.7 mA cm<sup>-2</sup>. The abatement of the catalyst concentration was fast and very similar with  
215 both anodes, attaining its total disappearance after 40–45 min of electrolysis, as can be observed  
216 in Fig. 1a. These trends confirm the large effectiveness of Fenton-like reaction (7) and, pre-  
217 eminently, photo-Fenton-like reaction (9), to form the most active species for H<sub>2</sub>O<sub>2</sub>  
218 decomposition, i.e., Fe(II)–EDDS and Fe<sup>2+</sup>. The slightly quicker disappearance occurred with  
219 the BDD anode can be ascribed to the larger reactivity of BDD(•OH) as compared to IrO<sub>2</sub>(•OH),  
220 produced via reaction (2) (Steter et al. 2016; Ridruejo et al. 2018). Both radicals might be able  
221 to attack the EDDS molecules, thus limiting the regeneration of the Fe(III)–EDDS through  
222 reaction (8). In addition, in both cells, the •OH produced from reaction (8) can attack the EDDS  
223 molecules in a more significant manner. The inset panel of Fig. 1a shows the analogous and  
224 good linear profiles obtained from the pseudo-first-order kinetic analysis of the two  
225 concentration decays, allowing the determination of an apparent rate constant for the catalyst  
226 degradation ( $k_c$ ) of 0.11 min<sup>-1</sup> in both cases, with a squared correlation coefficient ( $R^2$ ) > 0.991.  
227 This behavior suggests the attack of a steady •OH content on the catalytic complex.

228 The •OH generation via reactions (8) and (3) was feasible as long as Fe(III)–EDDS  
229 persisted in solution, since it was a continuous source of Fe(II)–EDDS and Fe<sup>2+</sup>. From Fig. 1a,  
230 it can be deduced that at 45 min the initial complex had been completely converted into Fe(III)  
231 and oxidation products of EDDS. This was confirmed by determining the TOC removal from  
232 the catalyst solution (initial value of 7.2 mg L<sup>-1</sup>) for 300 min. Fig. 1b highlights that no  
233 mineralization occurred when only 0.06 mM EDDS (without Fe(III)) were treated by EO-H<sub>2</sub>O<sub>2</sub>  
234 with an IrO<sub>2</sub>-based anode, informing about the scarce oxidation ability of IrO<sub>2</sub>(•OH) and H<sub>2</sub>O<sub>2</sub>  
235 towards the chelator. In contrast, the same process with a BDD anode led to 38% TOC decay,

236 in agreement with the greater reactivity of BDD( $\bullet$ OH) with organics (Brillas 2014). Fig. 1b  
237 discloses a TOC reduction of 12% and 57% when the PEF process was applied using the IrO<sub>2</sub>-  
238 based and BDD anode, respectively. The enhanced mineralization in PEF can then be attributed  
239 to the action of  $\bullet$ OH in the bulk, as explained above, which acted in concomitance with the UV  
240 photons on some Fe(III)-carboxylate byproducts (see reaction (6)).

241 In conclusion, the main oxidizing agents from ~45 min of electrolysis were: (i) M( $\bullet$ OH) at  
242 the anode surface, and (ii)  $\bullet$ OH produced from Fenton's reaction (3), mainly induced by photo-  
243 Fenton reaction (5). The amount of the latter radical was presumably small because the  
244 uncomplexed Fe(III) tended to precipitate at pH 7.0, thus being presumably critical the role of  
245 UVA light to photodecompose the generated products.

246 Comparative removal of triclopyr by EAOPs in sulfate medium

247 In a second step, triclopyr solutions at a concentration of 0.12 mM (10 mg L<sup>-1</sup> TOC) were  
248 prepared in sulfate medium, in the presence of 0.06 mM EDDS to be treated by EO-H<sub>2</sub>O<sub>2</sub> or  
249 0.06 mM Fe(III)-EDDS (1:1) for EF and PEF trials. A very different catalyst content decay can  
250 be seen in Fig. 2a during the two latter treatments at pH 7.0 and  $j = 16.7$  mA cm<sup>-2</sup>. In EF,  
251 Fe(III)-EDDS needed more than 300 min to disappear using an IrO<sub>2</sub>-based anode, whereas  
252 about 240 min were required with BDD. This agrees with the expected superior attack of  
253 BDD( $\bullet$ OH) on the catalyst. In contrast, a very fast Fe(III)-EDDS removal occurred in PEF,  
254 with complete abatement in 80 min regardless of the anode employed (see Fig. 2a). This  
255 suggests a high effectiveness of photo-Fenton-like reaction (9) for continuous generation of  
256 soluble Fe<sup>2+</sup>, originating  $\bullet$ OH from Fenton's reaction (3). From the excellent pseudo-first-order  
257 linear plots reported in Fig. 2b for such concentration decays, the  $k_c$ -value in EF with the IrO<sub>2</sub>-  
258 based anode exhibited a 2.6-fold increase when using BDD, approaching to a tenfold rise when  
259 applying PEF with both anodes (see Table 1). However, this rate constant was 0.43-fold lower

260 than that found in the absence of the herbicide (see Fig. 1a). This means that the generated  
261 oxidants participated not only in the abatement of Fe(III)–EDDS, but also in the simultaneous  
262 destruction of triclopyr and its byproducts, as explained below.

263 Fig. 2c shows an increasing herbicide removal in the order: EO-H<sub>2</sub>O<sub>2</sub> with IrO<sub>2</sub> < EF with  
264 IrO<sub>2</sub> < EO-H<sub>2</sub>O<sub>2</sub> with BDD < EF with BDD ~PEF with IrO<sub>2</sub> < PEF with BDD. Table 1  
265 summarizes the percentage of herbicide disappearance after a given electrolysis time in each  
266 process. Triclopyr concentration remained unaltered in EO-H<sub>2</sub>O<sub>2</sub> with the IrO<sub>2</sub>-based anode  
267 because of the low oxidation power of IrO<sub>2</sub>(•OH), whereas the formation of BDD(•OH)  
268 substantially upgraded the oxidation power of EO-H<sub>2</sub>O<sub>2</sub>. In fact, EO-H<sub>2</sub>O<sub>2</sub> with BDD  
269 outperformed the EF process with the IrO<sub>2</sub>-based anode, corroborating the key role of  
270 BDD(•OH) as compared to •OH originated from reaction (8). Similarly, the oxidation power of  
271 EF with BDD was similar to that of PEF with IrO<sub>2</sub>, despite the occurrence of photo-Fenton-like  
272 reaction (9) that ensured the Fe<sup>2+</sup> formation to feed Fenton's reaction (3). The conjunction of  
273 reactions (2), (3), (5) and (7)-(9) yielded sufficient amounts of BDD(•OH) and •OH that made  
274 the PEF with BDD the most effective process for triclopyr removal. The relative trends of all  
275 these processes agreed with the corresponding apparent rate constants for triclopyr decay (*k*<sub>1</sub>),  
276 gathered in Table 1, as calculated from the good kinetic analysis of Fig. 2d with *R*<sup>2</sup> > 0.993.

277 Analogous tendencies for the processes tested were also found for the corresponding TOC  
278 decays related to the mineralization of both, triclopyr and EDDS, as can be deduced from Fig.  
279 2e and the percentages of TOC removal at 300 min of electrolysis, collected in Table 1. It is  
280 noticeable that, once all the Fe(III)–EDDS was consumed, i.e., after 240 min in EF with BDD  
281 and 80 min in PEF with IrO<sub>2</sub> or BDD, the organics arisen from triclopyr and EDDS were mainly  
282 degraded by M(•OH), with a small contribution of •OH produced from a minimal concentration  
283 of soluble ferrous ions. In PEF, some final Fe(III)-carboxylate complexes were also  
284 photodecomposed via reaction (6). From the residual TOC at 300 min, it is evident that a

285 significant proportion of recalcitrant byproducts were accumulated, impeding the overall  
286 mineralization of the solutions. The most favorable conditions were then achieved in PEF with  
287 BDD, yielding 35% of accumulated TOC. In contrast, the last column of Table 1 reveals the  
288 smaller  $EC_{TOC}$  obtained in PEF with the  $IrO_2$ -based anode as compared to PEF with BDD (0.88  
289 vs. 1.31 kWh (g TOC)<sup>-1</sup>), owing to the smaller  $E_{cell}$  value (4.0 vs. 8.8 V). This means that the  
290 use of the  $IrO_2$ /air-diffusion cell in PEF was more cost-effective despite its lower oxidation  
291 ability, thanks to the large contribution of UVA radiation. However, a much higher total  $EC_{TOC}$   
292 including the electric power needed by the lamp (27.3 vs. 19.2 kWh (g TOC)<sup>-1</sup>) was determined  
293 for the  $IrO_2$ /air-diffusion cell, owing to much smaller mineralization ability. This suggests that  
294 the latter cell can be more cost-effective in the SPEF process with free sunlight irradiation.

#### 295 Effect of experimental variables on PEF performance for triclopyr degradation

296 Once demonstrated that the BDD/air-diffusion cell led to the quickest destruction of the  
297 target pollutant and TOC using the Fe(III)–EDDS (1:1) complex in PEF, the effect of the  
298 concentration of the soluble chelated catalyst on the process performance was assessed. Two  
299 reasons justify the low Fe(III)–EDDS contents chosen: (i) the need to avoid an excessive  
300 increase of TOC from EDDS, since its presence complicated the mineralization, and (ii) the  
301 control of iron precipitation as the soluble complex is destroyed, thus minimizing the sludge  
302 production. Based on these considerations, the PEF treatment of 0.12 mM triclopyr solutions  
303 within the Fe(III)–EDDS concentration range of 0.03–0.09 mM at pH 7.0 was studied at  $j =$   
304 16.7 mA cm<sup>-2</sup>. Fig. 3a highlights a quite similar decay of the catalyst content in all cases, always  
305 disappearing at 80 min. The pseudo-first-order kinetic analysis of these results, presented in the  
306 inset of Fig. 3a, yielded good linear correlations with analogous  $k_c$ -values (see Table 1).  
307 Gradually greater Fe(III)–EDDS contents favored the formation of •OH from reactions (7)–(9)  
308 that could attack the EDDS but, in turn, the self-destruction reactions between radicals (i.e.,

309 parasitic reactions) was also stimulated. As a result, no significant influence of the catalyst  
310 content was found within the studied range. Accordingly, Fig. 3b depicts a similar herbicide  
311 abatement regardless of the catalyst content. A larger amount of  $\bullet\text{OH}$  was formed at 0.06 and  
312 0.09 mM, but the amount of parasitic reactions increased as well, not being effective in practice  
313 those additional radicals. This can also be observed in the analogous TOC decay found at all  
314 Fe(III)–EDDS concentrations (see Fig. 3c), close to 62–66% (see Table 1). Since the initial TOC  
315 became greater as the catalyst concentration increased, the amount of TOC abated was actually  
316 enhanced:  $9.0 \text{ mg L}^{-1}$  at 0.03 mM vs.  $12.9 \text{ mg L}^{-1}$  at 0.09 mM. This was also reflected in the  
317 lower  $\text{EC}_{\text{TOC}}$  value needed at the highest Fe(III)–EDDS content (see Table 1).

318 Further, the influence of applied  $j$  was assessed for the PEF treatment of solutions  
319 containing 0.12 mM herbicide, 0.050 M  $\text{Na}_2\text{SO}_4$  and 0.06 mM Fe(III)–EDDS (1:1) at pH 7.0  
320 and 35 °C. These experiments were performed with BDD, at an initial  $j$  of  $16.7 \text{ mA cm}^{-2}$  for 60  
321 min, conditions that ensured that 94% of the chelated catalyst had disappeared (see Fig. 3a) and  
322 hence, practically all the iron ions were either hydrated or precipitated. Thereafter, the treatment  
323 proceeded at a higher  $j$  of 33.3 or  $66.7 \text{ mA cm}^{-2}$  for 240 min. The compared data of Fig. 3b and  
324 4a disclose a progressive enhancement of triclopyr abatement as  $j$  became higher, with time for  
325 total removal decreasing from 180 to 120 min when changing from constant  $j$  ( $16.7 \text{ mA cm}^{-2}$ )  
326 to variable  $j_1$  (16.7)/ $j_2$  (66.7) (see Table 1). Similarly, Fig. 3c and 4b illustrate a larger  
327 mineralization with increasing  $j$ , and Table 1 shows that the greatest TOC removal of 75% was  
328 reached operating at 16.7 (60 min)/ $66.7$  (240 min)  $\text{mA cm}^{-2}$ . Moreover, this table also evidences  
329 that the latter treatment accounted for a very high  $\text{EC}_{\text{TOC}}$  of  $10.02 \text{ kWh (g TOC)}^{-1}$ , as result of  
330 the high  $E_{\text{cell}}$  of 8.8/17.2 V. The improved oxidation ability derived from a greater applied  $j$  can  
331 be mainly related to the faster production of BDD( $\bullet\text{OH}$ ) from reaction (2), becoming the pre-  
332 eminent radical as Fe(III)–EDDS was degraded. A total soluble Fe content close to 0.03 mM  
333 was detected in the medium, similar to 0.04 mM permitted in natural water (Moreira et al.

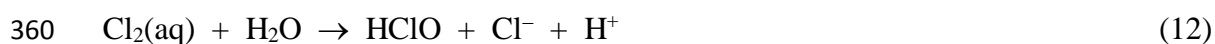
334 2015). This low amount of soluble iron served to promote the production of  $\bullet\text{OH}$ . Note that the  
335 rest of the Fe content initially dissolved was precipitated, deposited as  $\text{Fe}(\text{OH})_3$  at the cathode  
336 surface due to the strong alkalinity in its vicinity.

337 The fate of the heteroatoms of the herbicide (0.12 mM N, 0.36 mM Cl) and EDDS (0.12  
338 mM N) was assessed at the end of the PEF treatment with BDD at 16.7 (60 min)/33.3 (240 min)  
339  $\text{mA cm}^{-2}$ . Concentrations of 0.260 mM of  $\text{Cl}^-$  (72% of initial Cl) and 0.075 mM of  $\text{ClO}_3^-$  (21%  
340 of initial Cl), with traces of  $\text{ClO}_4^-$ , as well as 0.043 mM of  $\text{NO}_3^-$  (18% of total N) and 0.125  
341 mM of  $\text{NH}_4^+$  (52% of total N) were determined. These results agree with the complete release  
342 of heteroatoms as inorganic ions, which allows discarding the presence of a high amount of  
343 toxic chloro-organics in the residual TOC (Fig. 4b). The nitrogenated ions were also measured  
344 at the end of the EO- $\text{H}_2\text{O}_2$  treatment of 0.06 mM EDDS with BDD at  $j = 16.7 \text{ mA cm}^{-2}$ , only  
345 revealing the formation of 0.053 mM of  $\text{NO}_3^-$  (44% of initial N). It can be inferred that the  
346 pyridine group of the herbicide was the source of all the  $\text{NH}_4^+$  ion found.

#### 347 Treatment of triclopyr solutions by PEF in a mixed sulfate + chloride medium

348 Natural water and urban wastewater contain high quantities of  $\text{Cl}^-$  ion. To explore the  
349 influence of this anion on the PEF treatment of triclopyr with Fe(III)-EDDS, several trials were  
350 run in a matrix composed of 0.025 mM  $\text{Na}_2\text{SO}_4$  + 0.035 mM  $\text{NaCl}$ . The two salts were mixed  
351 in such proportion in order to ensure the same conductivity shown by the 0.050 M  $\text{Na}_2\text{SO}_4$   
352 solutions (Steter et al. 2016). In these treatments, the formation of  $\text{Cl}_2$  from  $\text{Cl}^-$  oxidation at the  
353 anode surface via reaction (11), followed by hydrolysis to hypochlorous acid at pH between 3.0  
354 and 8.0 via reaction (12) (Martínez-Huitle et al. 2015), is expected. The occurrence of reaction  
355 (11) limits the ability of the anode to generate  $\text{M}(\bullet\text{OH})$  by reaction (2), which can be potentially  
356 counterbalanced by the contribution of the oxidant  $\text{HClO}$ . This was assessed under PEF  
357 conditions using either active  $\text{IrO}_2$ - (DSA- $\text{O}_2$ ) and  $\text{RuO}_2$ -based (DSA- $\text{Cl}_2$ ) anodes or the non-

358 active BDD one.



361 The progressive accumulation of  $\text{H}_2\text{O}_2$  during the PEF treatment of 0.12 mM herbicide  
362 solutions in the mixed electrolyte with 0.06 mM Fe(III)–EDDS at pH 7.0 and  $j = 25 \text{ mA cm}^{-2}$   
363 is depicted in Fig. 5a. Final concentrations of 4.2, 5.1 and 6.4 mM were obtained with the  $\text{IrO}_2$ -  
364 based,  $\text{RuO}_2$ -based and BDD anode, respectively. The excess of  $\text{H}_2\text{O}_2$  detected in solution  
365 prevented that Fenton's reaction (3) and Fenton-like reaction (8) could be limited by a lack of  
366 that reagent, thus ensuring the maximum formation of  $\bullet\text{OH}$ . An analogous behavior can be  
367 observed in Fig. 5b for active chlorine. The unreacted oxidant was gradually accumulated in  
368 the solution, attaining a maximum concentration of  $7.2 \text{ mg L}^{-1}$  at 300 min using the  $\text{RuO}_2$ -based  
369 anode that decayed down to  $5.5 \text{ mg L}^{-1}$  with BDD. This agrees with the larger ability reported  
370 for the DSA- $\text{Cl}_2$  to oxidize  $\text{Cl}^-$ , as compared to the other two anodes (Brillas and Martínez-  
371 Huitle 2015).

372 Surprisingly, the catalyst and herbicide decays shown in Fig. 5c and d, respectively, did  
373 not depend substantially on the anode nature. The Fe(III)–EDDS concentration disappeared at  
374 about 120 min, a much longer time than that found in sulfate medium at  $j = 16.7 \text{ mA cm}^{-2}$  (80  
375 min, Fig. 2a), whereas triclopyr was removed at 90 min, a quite short time compared to that  
376 required in sulfate matrix (180 min, Fig. 2b). These findings, along with the similar  $k_c$  and  $k_1$   
377 values determined from the kinetic analysis presented in the inset panels of Fig. 5c and d and  
378 given in Table 2, suggest that the main oxidant of both organics (the chelator and the herbicide)  
379 was the active chlorine, rather than  $\text{M}(\bullet\text{OH})$  and  $\bullet\text{OH}$  mentioned in the sulfate one. As compared  
380 to those radicals, active chlorine reacted more slowly with Fe(III)–EDDS, but it was more  
381 effective to degrade triclopyr. Fig. 5e illustrates that the oxidation products were progressively



382 mineralized in this medium, reaching a large TOC abatement close to that found in sulfate  
383 medium when using BDD. This result is indicative of the participation of reactive BDD( $\bullet$ OH),  
384 whose oxidation power was greater than that of RuO<sub>2</sub>( $\bullet$ OH) and IrO<sub>2</sub>( $\bullet$ OH). However, it is clear  
385 from the EC<sub>TOC</sub> values of Table 2 that the treatment with the IrO<sub>2</sub>-based anode was preferred,  
386 despite yielding the lowest mineralization (65%). Without considering the energy consumption  
387 for light irradiation, i.e., under SPEF conditions, it was less energy-demanding thanks to the  
388 lower  $E_{\text{cell}}$  of 4.0 V as compared to 4.4 V with the RuO<sub>2</sub>-based anode and 8.8 V with BDD.

389 SPEF process in sulfate and mixed sulfate + chloride media

390 The removal of triclopyr at a concentration of 0.12 mM from solutions containing 0.050 M  
391 Na<sub>2</sub>SO<sub>4</sub> and 0.06 mM Fe(III)–EDDS (1:1) at pH 7.0 was finally assessed by SPEF as a cheap  
392 alternative to PEF. The study was made by comparing the behavior of an IrO<sub>2</sub>-based or BDD  
393 anode at  $j = 16.7 \text{ mA cm}^{-2}$ . Fig. 6a evidences a clear difference in their performance referred to  
394 the herbicide decay, showing a much faster disappearance using BDD. Total removal was  
395 achieved at 80 min, a much shorter time than in the case of the active anode (210 min). Note  
396 that these abatements were much quicker than those found during the analogous PEF treatments  
397 with a 6 W UVA lamp (180 and 270 min, respectively, see Fig. 2c). The superiority of BDD  
398 can be again related to the greater reactivity of BDD( $\bullet$ OH) as compared to IrO<sub>2</sub>( $\bullet$ OH), with  
399 similar quantities of both radicals being produced in PEF and SPEF. Regarding the process  
400 enhancement when sunlight replace UVA light, it can be ascribed to the much greater intensity  
401 of the photons of the former light source, thereby increasing the rate of the photolytic reactions  
402 (5) and (9) that accelerated the formation of  $\bullet$ OH from Fenton's reaction (3). The kinetic  
403 analysis of the above herbicide decays only allowed describing a pseudo-first-order reaction in  
404 the case of BDD, as can be seen in the inset of Fig. 6a. The  $k_1$ -value thus obtained in SPEF was  
405 2.7-fold greater than that determined in PEF (see Table 1). However, the TOC decays presented

406 in Fig. 6b in both SPEF systems were analogous to PEF ones shown in Fig. 2e. This means that,  
407 at long electrolysis time, once all the Fe(III)–EDDS catalyst has been destroyed and a small  
408 amount of uncomplexed iron ions is dissolved in the medium, the mineralization of byproducts  
409 by oxidant  $\bullet\text{OH}$  formed via reactions (3) and (5) or the photodecomposition of their Fe(III)  
410 complexes were the main routes using the  $\text{IrO}_2$ -based anode. In contrast, the contribution of  
411 BDD( $\bullet\text{OH}$ ) to the destruction of such byproducts seems much more relevant. In both types of  
412 cells, similar final TOC reductions and  $\text{EC}_{\text{TOC}}$  values were obtained in PEF and SPEF (see  
413 Table 1). This is a positive feature for the potential implementation of Fe(III)–EDDS-catalyzed  
414 SPEF treatment of pesticides in wastewater at larger scale. It is important to mention that in all  
415 the SPEF treatments the effect of direct solar photolysis on the pesticide degradation can be  
416 neglected. Several authors have shown that triclopyr has a long lifetime (as compared to the  
417 duration needed in the SPEF trials) in natural water under sunlight irradiation (Woodburn et al.  
418 1993).

419 The effect of  $j$  on the performance of SPEF process was examined in the same manner  
420 described on Fig. 4b for PEF, i.e., by applying a  $j = 16.7 \text{ mA cm}^{-2}$  for 60 min, whereupon it was  
421 increased to 33.33 or 66.7  $\text{mA cm}^{-2}$  for 240 min. Fig. 7 discloses the increase in TOC reduction  
422 as  $j$  became higher, reaching final values similar to those of PEF (see Table 1). A maximal of  
423 78% mineralization with an  $\text{EC}_{\text{TOC}} = 9.07 \text{ kWh (g TOC)}^{-1}$  was found in the treatment at 16.7  
424 (60 min)/66.7 (240 min)  $\text{mA cm}^{-2}$ . Under these conditions, Fig. 7 and Table 2 also highlight a  
425 similar performance in the 0.025 mM  $\text{Na}_2\text{SO}_4 + 0.035 \text{ mM NaCl}$  matrix. All these findings  
426 suggest that the rise in  $j$  pre-eminently favors the formation of oxidants at the BDD electrode,  
427 namely BDD( $\bullet\text{OH}$ ) from reaction (2) and/or  $\text{HClO}$  from reactions (11) and (12), with minor  
428 influence on the photolytic reactions.

429 One can conclude that the Fe(III)–EDDS-catalyzed PEF and SPEF treatments of triclopyr  
430 involve a complex mechanism. On the one hand,  $\text{M}(\bullet\text{OH})$  and/or  $\text{HClO}$  are produced and

431 oxidize both, the pesticide and the complex. On the other hand, the Fe(III)–EDDS complex  
432 reacts with the electrogenerated H<sub>2</sub>O<sub>2</sub> to yield •OH in the bulk from reactions (7) and (8). The  
433 role of light irradiation is quite significant, since it ensures the continuous generation of Fe<sup>2+</sup>  
434 from reaction (9). This ion can then form more •OH from Fenton’s reaction (3), alongside Fe<sup>3+</sup>  
435 that can be photoreduced to Fe<sup>2+</sup> from reaction (5), eventually increasing the amount of •OH.  
436 Additionally, the produced Fe<sup>2+</sup>/Fe<sup>3+</sup> ions can be complexed by the EDDS molecules or by  
437 several byproducts. When such iron complexes are photoactive, as in the case of some final  
438 carboxylic acids, they are photodecomposed, e.g., via reaction (6), enhancing the global  
439 mineralization process.

#### 440 Detection of byproducts

441 Table 3 collects the chemical name and structure, type of column, retention time and main  
442 fragments for the eight products detected after 40 min of electrolysis of a 0.12 mM triclopyr  
443 solution with 0.06 mM Fe(III)–EDDS solution in sulfate medium at pH 7.0 and  $j = 16.7 \text{ mA}$   
444  $\text{cm}^{-2}$ , under PEF conditions with BDD. All the byproducts identified by GC-MS, which are  
445 expected to be the same in SPEF, could only arise from the herbicide structure, i.e., no primary  
446 byproducts of EDDS were identified. Note that the possible products formed during the  
447 photodegradation of the Fe(III)–EDDS complex have been recently reported by Jaber et al.  
448 (2020). Based on our results, one can propose that triclopyr (**1**) was hydroxylated upon the  
449 attack of hydroxyl radicals either over the C(2) and C(3) positions of the pyridine ring to form  
450 the compound **2** with loss of Cl<sup>-</sup>, or over its C(1) atom to yield the derivative **4** with release of  
451 the lateral oxyacetic group. It is noteworthy that compound **4** has been reported as the main  
452 byproduct of **1** during its oxidation by TiO<sub>2</sub>/UV photocatalysis (Qamar et al. 2006) and by EO  
453 with BDD (Janíková-Bandžuchová et al. 2015). Further hydroxylation on the C(4) position of  
454 the heterocycle with release of Cl<sup>-</sup> and decarboxylation with hydroxylation of the oxyacetic

455 group produced the chloro-heteroaromatic **3**. The subsequent cleavage of the heterocycle ring  
456 of the above compounds led to two hydroxylated aliphatic byproducts, the aminobutyric acid **5**  
457 and the chloromethylene-propenimidic acid **6**. Dechlorination and hydroxylation of **6**,  
458 alongside the keto-enol tautomerism yielded the hydroxymethyl-malonamic acid **7**, whereas the  
459 loss of the -CH<sub>2</sub>OH-COOH group upon hydroxylation of **7** yielded the carbamic acid **8**. Finally,  
460 decarboxylation of **8** with oxidation of the hydroxymethyl group resulted in formamide **9**. From  
461 the detected byproducts, a degradation route for **1** by PEF and SPEF is proposed in Fig. 8.

462 The production of short-chain carboxylic acids before total mineralization of aromatic and  
463 heteroaromatic pollutants is expected in Fenton-based processes. These compounds tend to  
464 form Fe(III) complexes (Martínez-Huitle et al. 2015). To confirm this, solutions with 0.12 mM  
465 triclopyr and 0.06 mM Fe(III)-EDDS in 0.050 M Na<sub>2</sub>SO<sub>4</sub> at pH 7.0 were treated by PEF and  
466 SPEF using the BDD/air-diffusion cell at  $j = 16.7 \text{ mA cm}^{-2}$  and analyzed for 300 min by ion-  
467 exclusion HPLC. Tartronic acid (**10**) coming from longer aliphatic carboxylic acids and oxamic  
468 acid (**11**) proceeding from *N*-derivatives were detected. In PEF, only traces of **10** were found,  
469 whereas **11** was accumulated up to 4.0 mg L<sup>-1</sup> (1.1 mg L<sup>-1</sup> TOC), as shows Fig. 9a. In the case  
470 of SPEF, Fig. 9b discloses a maximum accumulation of 3.5 mg L<sup>-1</sup> for **10**, disappearing at 300  
471 min, and of 5.7 mg L<sup>-1</sup> for **11**, dropping down up to 1.6 mg L<sup>-1</sup> (0.4 mg L<sup>-1</sup> TOC). The small  
472 quantity of the two byproducts, as compared to 6.0-6.5 mg L<sup>-1</sup> TOC found in the final solutions  
473 treated by PEF (see Fig. 2e) and SPEF (see Fig. 6b) suggests the generation of recalcitrant  
474 undetected byproducts. Fig. 9a and b demonstrate a remarkable influence of the light source on  
475 the profile of the concentrations of the acids. The illumination with sunlight in SPEF accelerated  
476 the production and destruction of the Fe(III) complexes of **10** and **11**. Hence, the action of  
477 photons is denoted in the final step of the route of Fig. 8, aiming to explain better the  
478 mineralization of **1** by both, PEF and SPEF treatments.

## 479 **Conclusions**

480 The Fe(III)–EDDS (1:1) complex was proven an efficient iron catalyst for treating the  
481 herbicide triclopyr at pH 7.0 by PEF process. A catalyst content as low as 0.06 mM performed  
482 quite well, although it was gradually destroyed under the action of M( $\bullet$ OH),  $\bullet$ OH and, pre-  
483 eminently, UV photons, yielding some soluble uncomplexed iron ions that originated  $\bullet$ OH from  
484 conventional Fenton's reaction. Triclopyr degradation and TOC decay were enhanced using  
485 BDD anode, although the treatment was less expensive with the IrO<sub>2</sub>-based one. Similar  
486 catalyst, herbicide and TOC removals were obtained within the range 0.03-0.09 mM Fe(III)–  
487 EDDS. The increasing production of BDD( $\bullet$ OH) as  $j$  became higher enhanced the TOC  
488 abatement once all the chelated catalyst had disappeared. The PEF experiments performed in  
489 0.25 mM Na<sub>2</sub>SO<sub>4</sub> + 0.35 mM NaCl revealed a large influence of active chlorine as oxidant. The  
490 SPEF process with BDD yielded better results than PEF for triclopyr removal due to the larger  
491 photon intensity from sunlight, but the TOC abatement was similar in both systems, attaining a  
492 maximal of 78% at  $j = 66.7 \text{ mA cm}^{-2}$ . Three heteroaromatics, four linear *N*-aliphatics and  
493 formamide were detected as byproducts of triclopyr. Tartronic and oxamic acids appeared as  
494 final short-chain carboxylic acids, being more rapidly destroyed in SPEF.

## 495 **Authors' contributions**

496 Conceptualization: Z.H. Ye, I. Sirés; Formal analysis and investigation: I.C. Da Costa Soares, Z.H.  
497 Ye, R. Oriol; Funding acquisition: I. Sirés, P.L. Cabot, C.A. Martínez-Huitle; Methodology: Z.H. Ye, I.  
498 Sirés; Resources: I. Sirés, E. Brillas; Supervision: I. Sirés, C.A. Martínez-Huitle; Writing—original draft  
499 preparation: I. Sirés, E. Brillas; Writing review and editing: all authors read and approved the final  
500 manuscript.

## 501 **Funding**

502 The authors thank financial support from projects CTQ2016-78616-R (AEI/FEDER, EU),  
503 PID2019-109291RB-I00 (AEI, Spain), CNPq – 439344/2018-2 (Conselho Nacional de  
504 Desenvolvimento Científico e Tecnológico, Brazil) and FAPESP project 2014/50945-4 (Fundação de  
505 Amparo à Pesquisa do Estado de São Paulo, Brazil), as well as the PhD scholarships awarded to I.C. Da  
506 Costa Soares (CNPq 200009/2018-4, Brazil), Z. Ye (State Scholarship Fund, CSC, China) and R. Oriol  
507 (MINECO, Spain).

#### 508 **Data availability**

509 The datasets used and/or analyzed during the current study are available from the corresponding  
510 author on reasonable request.

#### 511 **Compliance with ethical standards**

#### 512 **Competing interests**

513 The authors declare that they have no competing interests.

#### 514 **Ethical approval**

515 Not applicable.

#### 516 **Consent to participate**

517 Not applicable.

#### 518 **Consent to publish**

519 Not applicable.

#### 520 **References**

521 APHA, AWWA, WEF (2005) Standard Methods for the Examination of Water and

522 Wastewater, 21st Ed. Method Number 4500-Cl Chlorine (residual)–G. DPD Colorimetric  
523 Method, American Public Health Association, Washington D.C., pp. 4–67 and 4–68.

524 Battaglin WA, Rice KC, Focazio MJ, Salmons S, Barry RX (2009) The occurrence of  
525 glyphosate, atrazine, and other pesticides in vernal pools and adjacent streams in  
526 Washington, DC, Maryland, Iowa, and Wyoming, 2005-2006. *Environ Monit Assess*  
527 155:281–307. <https://doi.org/10.1007/s10661-008-0435-y>

528 Brillas E (2014) A review on the degradation of organic pollutants in waters by UV  
529 photoelectro-Fenton and solar photoelectro-Fenton. *J Braz Chem Soc* 25:393–417.  
530 <https://doi.org/10.5935/0103-5053.20130257>

531 Brillas E, Martínez-Huitle CA (2015) Decontamination of wastewaters containing synthetic  
532 organic dyes by electrochemical methods. An updated review. *Appl Catal B: Environ*  
533 166–167:603–643. <https://doi.org/10.1016/j.apcatb.2014.11.016>

534 Clarizia L, Russo D, Di Somma I, Marotta R, Andreozzi R (2017) Homogeneous photo-Fenton  
535 processes at near neutral pH: a review. *Appl Catal B: Environ* 209:358–371.  
536 <https://doi.org/10.1016/j.apcatb.2017.03.011>

537 Clematis D, Cerisola G, Panizza M (2017) Electrochemical oxidation of a synthetic dye using  
538 a BDD anode with a solid polymer electrolyte. *Electrochem Commun* 75:21–24.  
539 <https://doi.org/10.1016/j.elecom.2016.12.008>

540 Edginton AN, Stephenson GR, Sheridan PM, Thompson DG, Boermans HJ (2003) Effect of  
541 pH and release on two life stages of four anuran amphibians. *Environ Toxicol Chem*  
542 22:2673–2678. <https://doi.org/10.1897/02-484>

543 El-Ghenymy A, Rodríguez RM, Brillas E, Oturan N, Oturan MA (2014) Electro-Fenton  
544 degradation of the antibiotic sulfanilamide with Pt/carbon-felt and BDD/carbon-felt cells.  
545 Kinetics, reaction intermediates, and toxicity assessment. *Environ Sci Pollut Res*  
546 21:8368–8378. <https://doi.org/10.1007/s11356-014-2773-3>

547 El-Ghenymy A, Centellas F, Rodríguez RM, Cabot, PL, Garrido JA, Sirés I, Brillas E (2015)  
548 Comparative use of anodic oxidation, electro-Fenton and photoelectro-Fenton with Pt or  
549 boron-doped diamond anode to decolorize and mineralize Malachite Green oxalate dye.  
550 *Electrochim Acta* 182:247–256. <https://doi.org/10.1016/j.electacta.2015.09.078>

551 Galia A, Lanzalaco S, Sabatino MA, Dispenza C, Scialdone O, Sirés I (2016) Crosslinking of  
552 poly(vinylpyrrolidone) activated by electrogenerated hydroxyl radicals: a first step  
553 towards a simple and cheap synthetic route of nanogel vectors. *Electrochem Commun*  
554 62:64–68. <https://doi.org/10.1016/j.elecom.2015.12.005>

555 Ganiyu SO, Zhou M, Martínez-Huitle CA (2018) Heterogeneous electro-Fenton and  
556 photoelectro-Fenton processes: a critical review of fundamental principles and  
557 application for water/wastewater treatment. *Appl Catal B: Environ* 235:103–129.  
558 <https://doi.org/10.1016/j.apcatb.2018.04.044>

559 Ganzenko O, Oturan N, Sirés I, Huguenot D, van Hullebusch ED, Esposito G, Oturan MA  
560 (2018) Fast and complete removal of the 5-fluorouracil drug from water by electro-Fenton  
561 oxidation. *Environ Chem Lett* 16:281–286. <https://doi.org/10.1007/s10311-017-0659-6>

562 Jaber S, Lereboure M, They V, Delort A-M, Mailhot G (2020) Mechanism of photochemical  
563 degradation of Fe(III)-EDDS complex. *J Photochem Photobiol A: Chem* 399:112646.  
564 <https://doi.org/10.1016/j.jphotochem.2020.112646>

565 Janíková-Bandžuchová L, Šelešovská R, Schwarzová-Pecková K, Chýlková J (2015) Sensitive  
566 voltammetric method for rapid determination of pyridine herbicide triclopyr on bare  
567 boron-doped diamond electrode. *Electrochim Acta* 154:421–429.  
568 <https://doi.org/10.1016/j.electacta.2014.12.064>

569 Lanzalaco S, Sirés I, Sabatino MA, Dispenza C, Scialdone O, Galia A (2017) Synthesis of  
570 polymer nanogels by electro-Fenton process: investigation of the effect of main operation  
571 parameters. *Electrochim Acta* 246:812–822.



572 <https://doi.org/10.1016/j.electacta.2017.06.097>

573 Lanzalaco S, Sirés I, Galia A, Sabatino MA, Dispenza C, Scialdone O (2018) Facile  
574 crosslinking of poly(vinylpyrrolidone) by electro-oxidation with IrO<sub>2</sub>-based anode under  
575 potentiostatic conditions. *J Appl Electrochem* 48:1343–1352.  
576 <https://doi.org/10.1007/s10800-018-1237-8>

577 Lei W, Tang X, Zhou X (2018) Transport of 3,5,6-trichloro-2-pyridinol (a main pesticide  
578 degradation product) in purple soil: experimental and modeling. *Appl Geochem* 88:179–  
579 187. <https://doi.org/10.1016/j.apgeochem.2017.07.010>

580 Li W, Mao J, Dai X, Zhao X, Qiao C, Zhang X, Pu E (2018) Residue determination of triclopyr  
581 and aminopyralid in pastures and soil by gas chromatography-electron capture detector:  
582 dissipation pattern under open field conditions. *Ecotoxicol Environ Saf* 155:17–25.  
583 <https://doi.org/10.1016/j.ecoenv.2018.02.035>

584 Maddila S, Rana S, Pagadala R, Maddila SN, Vasam C, Jonnalagadda SB (2015) Ozone-driven  
585 photocatalyzed degradation and mineralization of pesticide triclopyr by Au/TiO<sub>2</sub>. *J*  
586 *Environ Sci Health B* 50:571–583. <https://doi.org/10.1080/03601234.2015.1028835>

587 Martínez-Huitle CA, Panizza M (2018) Electrochemical oxidation of organic pollutants for  
588 wastewater treatment. *Curr Opin Electrochem* 11:62–71.  
589 <https://doi.org/10.1016/j.coelec.2018.07.010>

590 Martínez-Huitle CA, Rodrigo MA, Sirés I, Scialdone O (2015) Single and coupled  
591 electrochemical processes and reactors for the abatement of organic water pollutants: a  
592 critical review. *Chem Rev* 115:13362–13407.  
593 <https://doi.org/10.1021/acs.chemrev.5b00361>

594 Miralles-Cuevas S, Oller I, Ruíz-Delgado A, Cabrera-Reina A, Cornejo-Ponce L, Malato S  
595 (2019) EDDS as complexing agent for enhancing solar advanced oxidation processes in  
596 natural water: effect of iron species and different oxidants. *J Hazard Mater* 372:129–136.

597 <https://doi.org/10.1016/j.jhazmat.2018.03.018>

598 Moreira FC, Boaventura RAR, Brillas E, Vilar VJP (2015) Degradation of trimethoprim  
599 antibiotic by UVA photoelectro-Fenton process mediated by Fe(III)–carboxylate  
600 complexes. *Appl Catal B: Environ* 162 (2015) 34–44.  
601 <http://dx.doi.org/10.1016/j.apcatb.2014.06.008>

602 Pérez T, Sirés I, Brillas E, Nava JL (2017) Solar photoelectro-Fenton flow plant modeling for  
603 the degradation of the antibiotic erythromycin in sulfate medium. *Electrochim Acta*  
604 228:45-56. <https://doi.org/10.1016/j.electacta.2017.01.047>

605 Pérez-Lucas G, Aliste M, Vela N, Garrido I, Fenoll J, Navarro S (2020) Decline of fluroxypyr  
606 and triclopyr residues from pure, drinking and leaching water by photo-assisted  
607 peroxonation. *Process Saf Environ Protec* 137:358–365.  
608 <https://doi.org/10.1016/j.psep.2020.02.039>

609 Qamar M, Muneer M, Bahnemann D (2006) Heterogeneous photocatalysed degradation of two  
610 selected pesticide derivatives, triclopyr and aminoimidazole in aqueous suspensions of titanium  
611 dioxide. *J Environ Manag* 80:99–106. <https://doi.org/10.1016/j.jenvman.2005.09.002>

612 Ridruejo C, Centellas F, Cabot PL, Sirés I, Brillas E (2018) Electrochemical Fenton-based  
613 treatment of tetracaine in synthetic and urban wastewater using active and non-active  
614 anodes. *Water Res* 128:71–81. <https://doi.org/10.1016/j.watres.2017.10.048>

615 Rippy MA, Deletic A, Black J, Aryal R, Lampard JL, Tang JYM, McCarthy D, Kolotelo P,  
616 Sidhu J, Gernjak W (2017) Pesticide occurrence and spatio-temporal variability in urban  
617 run-off across Australia. *Water Res* 115:245–255.  
618 <https://doi.org/10.1016/j.watres.2017.03.010>

619 Roth H, Gendel Y, Buzatu P, David O, Wessling M (2016) Tubular carbon nanotube-based gas  
620 diffusion electrode removes persistent organic pollutants by a cyclic adsorption – electro-  
621 Fenton process. *J Hazard Mater* 307:1–6. <https://doi.org/10.1016/j.jhazmat.2015.12.066>

622 Senseman SA (2007) *Herbicide Handbook*. 9th ed., Weed Society of America, USA.

623 Solís RR, Rivas FJ, Gimeno O, Pérez-Bote JL (2016) Photocatalytic ozonation of clopyralid,  
624 picloram and triclopyr. Kinetics, toxicity and influence of operational parameters. *J Chem*  
625 *Technol Biotechnol* 91:51–58. <https://doi.org/10.1002/jctb.4542>

626 Steter JR, Brillas E, Sirés I (2016) On the selection of the anode material for the electrochemical  
627 removal of methylparaben from different aqueous media. *Electrochim Acta* 222:1464–  
628 1474. <https://doi.org/10.1016/j.electacta.2016.11.125>

629 Thiam A, Sirés I, Brillas E (2015) Treatment of a mixture of food color additives (E122, E124  
630 and E129) in different water matrices by UVA and solar photoelectro-Fenton. *Water Res*  
631 81:178–187. <https://doi.org/10.1016/j.watres.2015.05.057>

632 Vasudevan S, Oturan MA (2014) Electrochemistry as cause and cure in water pollution. An  
633 overview. *Environ Chem Lett* 12:97–108. <https://doi.org/10.1007/s10311-013-0434-2>

634 Woodburn KB, Batzer FR, White FH, Schultz MR (1993) The aqueous photolysis of triclopyr.  
635 *Environ Toxicol Chem* 12:43–55. <https://doi.org/10.1002/etc.5620120107>

636 Yadav S, Kumar N, Kumari V, Mittal A, Sharma S (2019) Photocatalytic degradation of  
637 triclopyr, a persistent pesticide by ZnO/SnO<sub>2</sub> nano-composites. *Mater Today: Proc*  
638 19:642–645. <https://doi.org/10.1016/j.matpr.2019.07.746>

639 Yahya MS, Oturan N, El Kacemi K, El Karbane M, Aravindakumar CT, Oturan MA (2014)  
640 Oxidative degradation study on antimicrobial agent ciprofloxacin by electro-Fenton  
641 process: kinetics and oxidation products. *Chemosphere* 117:447–454.  
642 <https://doi.org/10.1016/j.chemosphere.2014.08.016>

643 Yang W, Zhou M, Oturan N, Li Y, Oturan MA (2019) Electrocatalytic destruction of  
644 pharmaceutical imatinib by electro-Fenton process with graphene-based cathode.  
645 *Electrochim Acta* 305:285–294. <https://doi.org/10.1016/j.electacta.2019.03.067>

646 Ye Z, Brillas E, Centellas F, Cabot PL, Sirés I (2019a) Electro-Fenton process at mild pH using

647 Fe(III)–EDDS as soluble catalyst and carbon felt as cathode. *Appl Catal B: Environ*  
648 257:117907. <https://doi.org/10.1016/j.apcatb.2019.117907>

649 Ye Z, Brillas E, Centellas F, Cabot PL, Sirés I (2020a) Expanding the application of  
650 photoelectro-Fenton treatment to urban wastewater using the Fe(III)–EDDS complex.  
651 *Water Res* 169:115219. <https://doi.org/10.1016/j.watres.2019.115219>

652 Ye Z., Guelfi DRV, Álvarez G, Alcaide F, Brillas E, Sirés I (2019b) Enhanced electrocatalytic  
653 production of H<sub>2</sub>O<sub>2</sub> at Co-based air-diffusion cathodes for the photoelectro-Fenton  
654 treatment of bronopol. *Appl Catal B: Environ* 247:191–199.  
655 <https://doi.org/10.1016/j.apcatb.2019.01.029>

656 Ye Z, Padilla JA, Xuriguera E, Beltran, JL, Alcaide F, Brillas E, Sirés I (2020b) A highly stable  
657 metal–organic framework-engineered FeS<sub>2</sub>/C nanocatalyst for heterogeneous electro-  
658 Fenton treatment: Validation in wastewater at mild pH. *Environ Sci Technol* 54:4664–  
659 4674. <https://dx.doi.org/10.1021/acs.est.9b07604>

660 Ye Z., Sirés I, Zhang H, Huang Y-H (2019c) Mineralization of pentachlorophenol by  
661 ferrioxalate-assisted solar photo-Fenton process at mild pH. *Chemosphere* 217:475–482.  
662 <https://doi.org/10.1016/j.chemosphere.2018.10.221>

663 Zhang Y, Klammerth N, Ashagre Messele S, Chelme-Ayala P, Gamal El-Din M (2016) Kinetics  
664 study on the degradation of a model naphthenic acid by ethylenediamine-*N,N'*-disuccinic  
665 acid-modified Fenton process. *J Hazard Mater* 318:371–378.  
666 <https://doi.org/10.1016/j.jhazmat.2016.06.063>

667

668 **Figure captions**

669 **Fig. 1** (a) Normalized concentration of the Fe(III)–EDDS (1:1) complex, with the  
670 corresponding kinetic analysis, and (b) normalized TOC vs. electrolysis time for the PEF  
671 treatment of 150 mL of solutions containing 0.06 mM catalyst (7.2 mg L<sup>-1</sup> TOC) and 0.050 M  
672 Na<sub>2</sub>SO<sub>4</sub> at pH 7.0 and 35 °C. A stirred tank reactor with an IrO<sub>2</sub>-based or a BDD anode and an  
673 air-diffusion cathode, both of 3 cm<sup>2</sup> area, was employed at current density (*j*) of 16.7 mA cm<sup>-2</sup>  
674 under irradiation with a 6 W UVA lamp. Plot (b) also includes the comparative EO-H<sub>2</sub>O<sub>2</sub>  
675 treatments made under the same conditions, with EDDS but without Fe(III).

676 **Fig. 2** Change of normalized (a) Fe(III)–EDDS (1:1) concentration, (c) triclopyr concentration  
677 and (e) TOC with electrolysis time for the treatment of 150 mL of solutions containing 0.12  
678 mM triclopyr (10.0 mg L<sup>-1</sup> TOC), 0.050 M Na<sub>2</sub>SO<sub>4</sub> and 0.06 mM (7.2 mg L<sup>-1</sup> TOC) catalyst at  
679 pH 7.0 and 35 °C, using a cell with an IrO<sub>2</sub>-based or BDD anode and an air-diffusion cathode  
680 (3 cm<sup>2</sup> electrode area each) at *j* = 16.7 mA cm<sup>-2</sup>. Method: EO-H<sub>2</sub>O<sub>2</sub> (with EDDS, no Fe(III))  
681 with (△) IrO<sub>2</sub>-based or (○) BDD, EF with (▽) IrO<sub>2</sub>-based or (□) BDD, and PEF with (▲)  
682 IrO<sub>2</sub>-based or (●) BDD. Plots (b) and (d) depict the pseudo-first-order kinetic analysis of curves  
683 shown in (a) and (c), respectively.

684 **Fig. 3** Effect of Fe(III)–EDDS (1:1) content over the time course of normalized (a) catalyst  
685 concentration, (b) triclopyr concentration and (c) TOC during the PEF treatment of 150 mL of  
686 solutions with 0.12 mM triclopyr (10.0 mg L<sup>-1</sup> TOC), 0.050 M Na<sub>2</sub>SO<sub>4</sub> and 0.03 mM (3.6 mg  
687 L<sup>-1</sup> TOC), 0.06 mM (7.2 mg L<sup>-1</sup> TOC) or 0.09 mM (10.8 mg L<sup>-1</sup> TOC) catalyst at pH 7.0 and  
688 35 °C, using a BDD/air-diffusion cell *j* = 16.7 mA cm<sup>-2</sup>. In (a,b), the inset panel presents the  
689 corresponding pseudo-first-order kinetic analysis.

690 **Fig. 4** Normalized (a) triclopyr concentration and (b) TOC vs. electrolysis time during the PEF  
691 treatment of 150 mL of solutions with 0.12 mM triclopyr (10.0 mg L<sup>-1</sup> TOC), 0.050 M Na<sub>2</sub>SO<sub>4</sub>  
692 and 0.06 mM (7.2 mg L<sup>-1</sup> TOC) Fe(III)–EDDS (1.1) at pH 7.0 and 35 °C, using a BDD/air-  
693 diffusion cell at applied *j* of (●) 16.7 mA cm<sup>-2</sup> for 60 min, followed by (◇) 33.3 mA cm<sup>-2</sup> or

694 (□) 66.7 mA cm<sup>-2</sup>.

695 **Fig. 5** Effect of the anode on the variation of the concentration of (a) accumulated H<sub>2</sub>O<sub>2</sub>, (b)  
696 active chlorine, (c) normalized Fe(III)–EDDS, (d) triclopyr and (e) TOC with electrolysis time  
697 for the PEF treatment of 150 mL of solutions containing 0.12 mM triclopyr (10.0 mg L<sup>-1</sup> TOC),  
698 0.025 M Na<sub>2</sub>SO<sub>4</sub> + 0.035 M NaCl and 0.06 mM (7.2 mg L<sup>-1</sup> TOC) Fe(III)–EDDS (1:1) at pH  
699 7.0, 35 °C and  $j = 25$  mA cm<sup>-2</sup>. In (c,d), the corresponding pseudo-first-order kinetic analysis is  
700 shown in the inset panel.

701 **Fig. 6** Variation of normalized (a) triclopyr concentration and (b) TOC with electrolysis time  
702 during the SPEF treatment of 150 mL of solutions with 0.12 mM herbicide (10.0 mg L<sup>-1</sup> TOC),  
703 0.050 M Na<sub>2</sub>SO<sub>4</sub> and 0.06 mM (7.2 mg L<sup>-1</sup> TOC) Fe(III)–EDDS (1:1) at pH 7.0 and 35 °C, using  
704 a cell with an IrO<sub>2</sub>-based or BDD anode and an air-diffusion cathode at  $j = 16.7$  mA cm<sup>-2</sup>.

705 **Fig. 7** TOC abatement vs. electrolysis time for the SPEF treatment of 150 mL of solutions with  
706 0.12 mM triclopyr (10.0 mg L<sup>-1</sup> TOC) and 0.06 mM Fe(III)–EDDS (1:1) (7.2 mg L<sup>-1</sup> TOC) at  
707 pH 7.0 and 35 °C, using a BDD/air-diffusion cell at  $j$  of (●) 16.7 mA cm<sup>-2</sup> for 60 min, followed  
708 by (◇) 33.3 mA cm<sup>-2</sup> and (□,▽) 66.7 mA cm<sup>-2</sup>. Electrolyte: (◇,□) 0.050 M Na<sub>2</sub>SO<sub>4</sub> and (▽)  
709 0.025 M Na<sub>2</sub>SO<sub>4</sub> + 0.035 M NaCl.

710 **Fig. 8** Proposed mineralization route for triclopyr by PEF and SPEF treatments under the action  
711 of hydroxyl radical and light. The name of byproducts is given in Table 3.

712 **Fig. 9** Evolution of the concentration of (▲) tartronic (**10**) and (■) oxamic (**11**) acids detected  
713 during the (a) PEF and (b) SPEF treatments of 150 mL of solutions with 0.12 mM triclopyr,  
714 0.050 M Na<sub>2</sub>SO<sub>4</sub> and 0.06 mM (7.2 mg L<sup>-1</sup> TOC) Fe(III)–EDDS (1:1) at pH 7.0 and 35 °C,  
715 using a BDD/air-diffusion cell at  $j = 16.7$  mA cm<sup>-2</sup> for 60 min, followed by 66.7 mA cm<sup>-2</sup>.

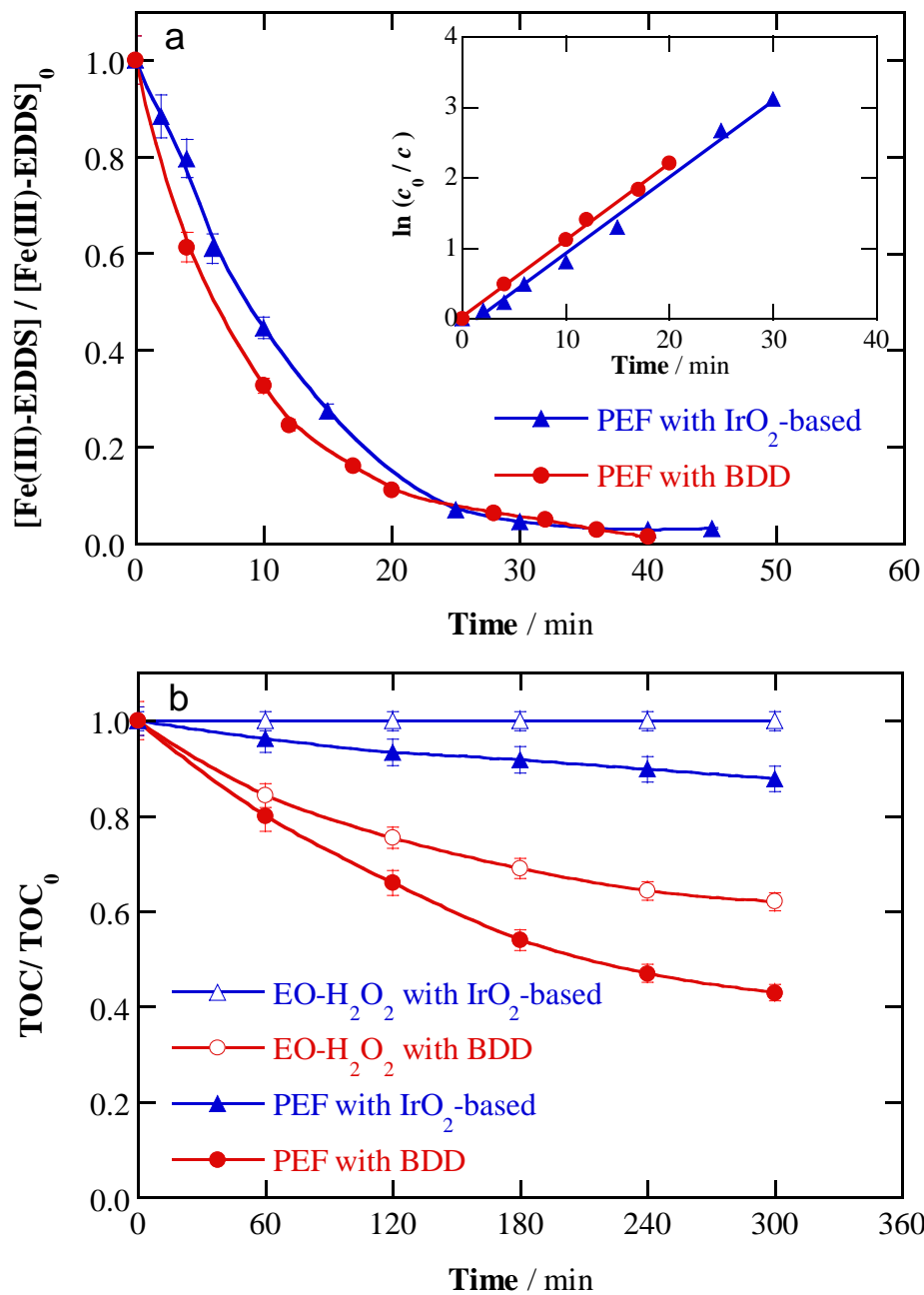


**Fig. 1**

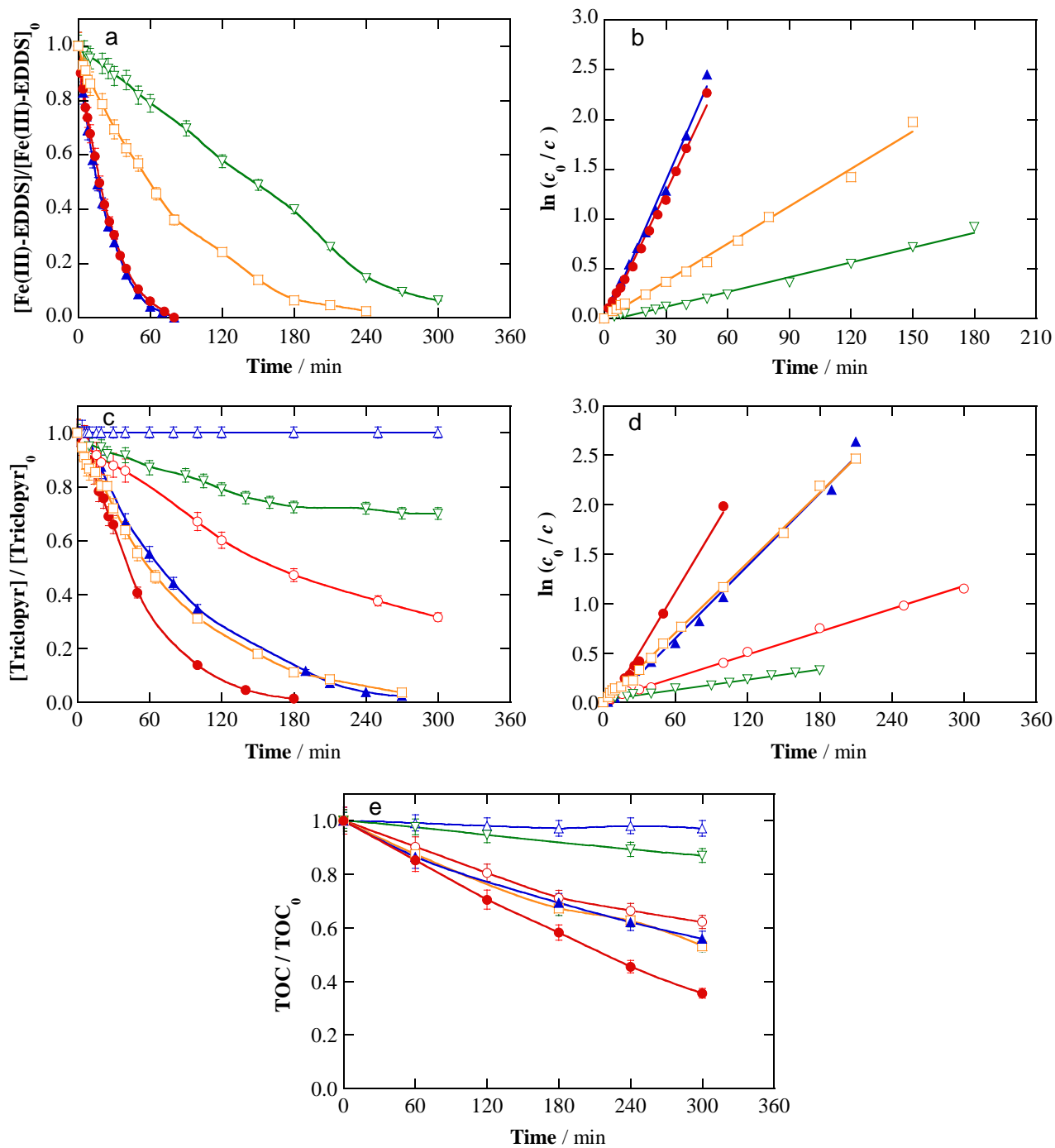


Fig. 2



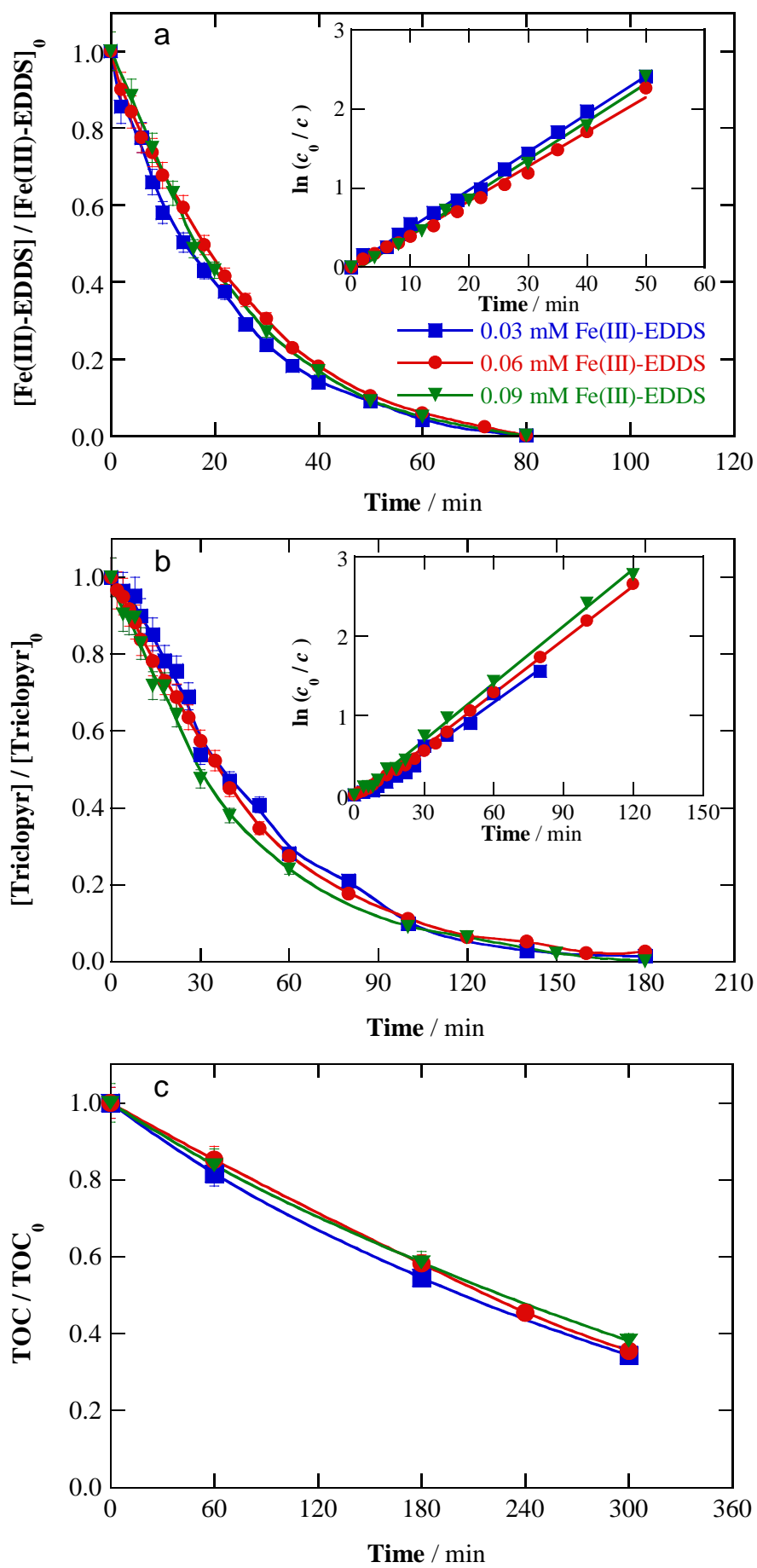


Fig. 3

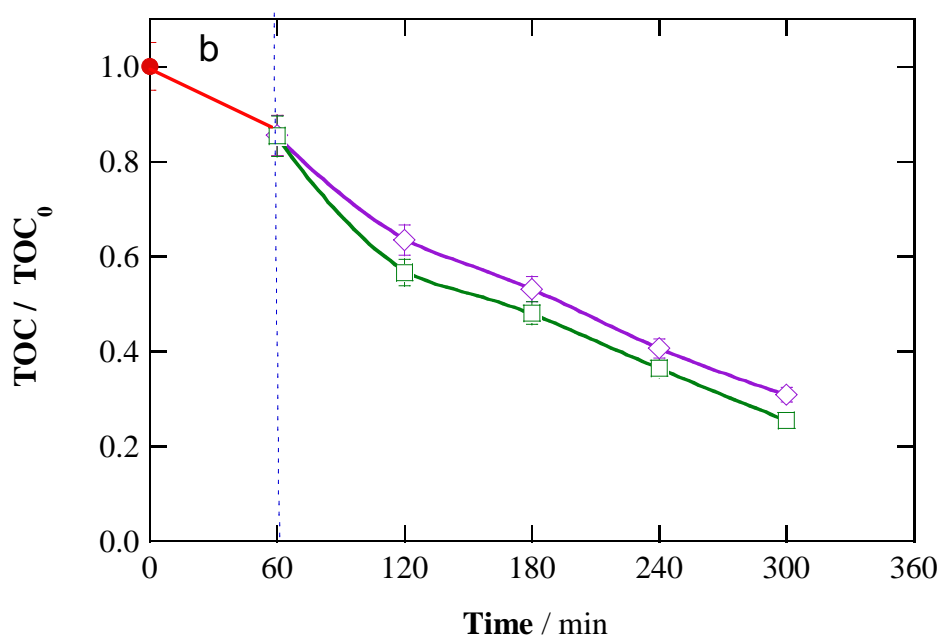
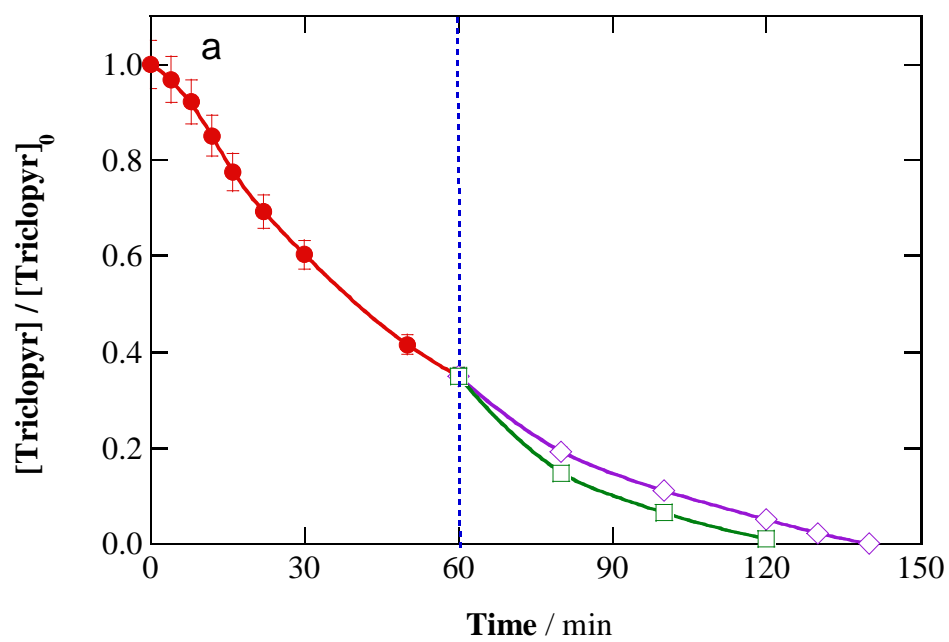


Fig. 4

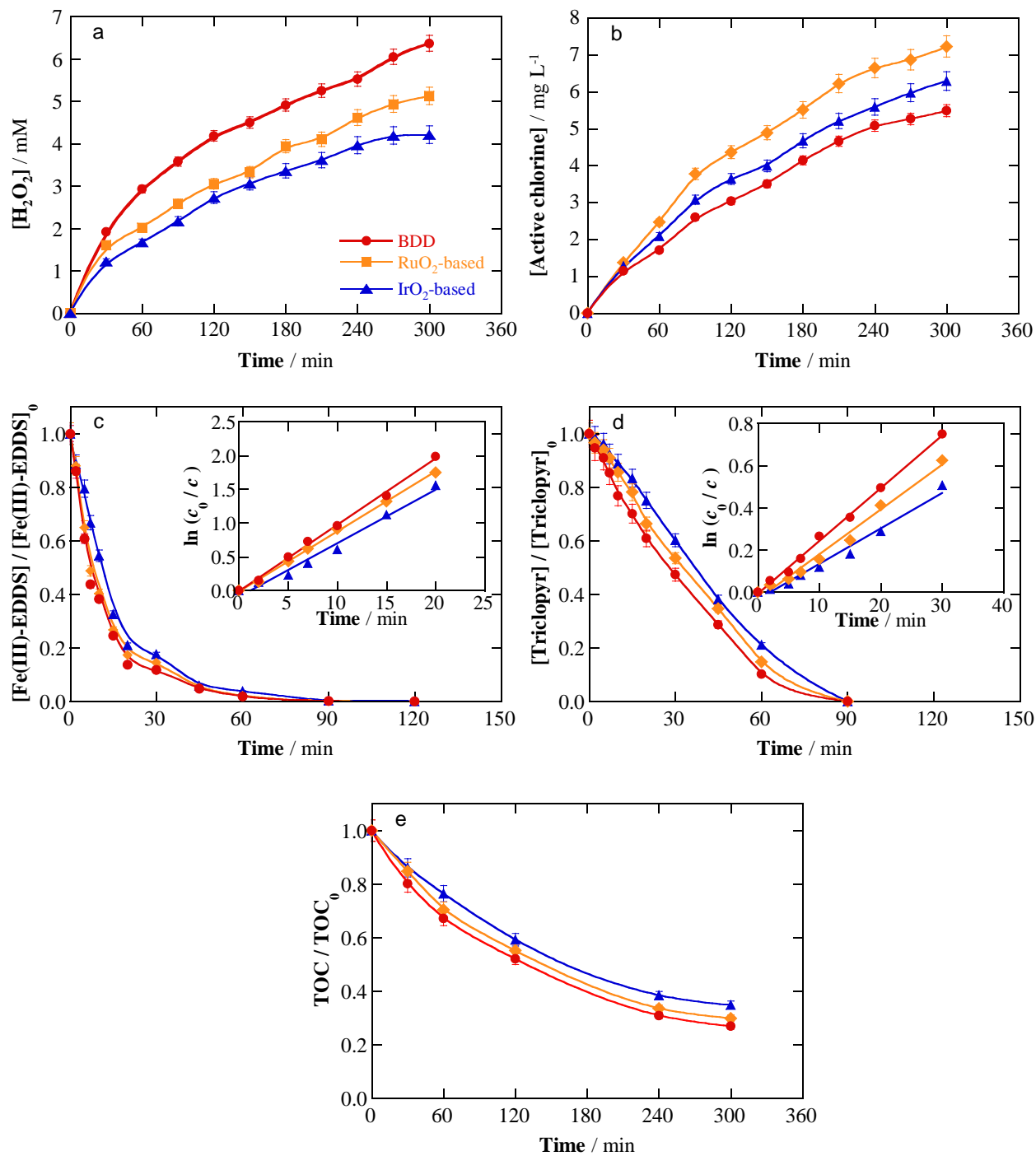
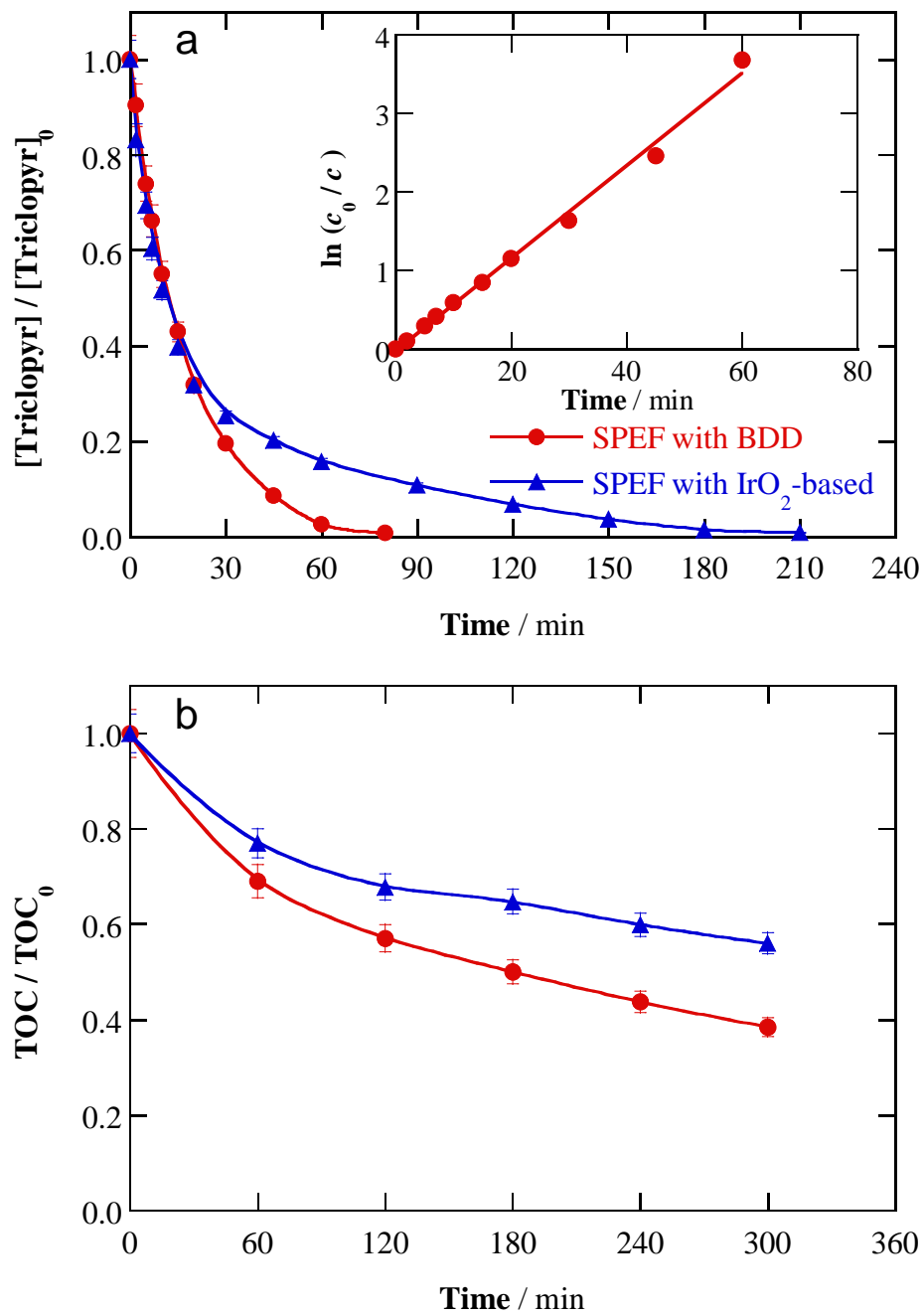
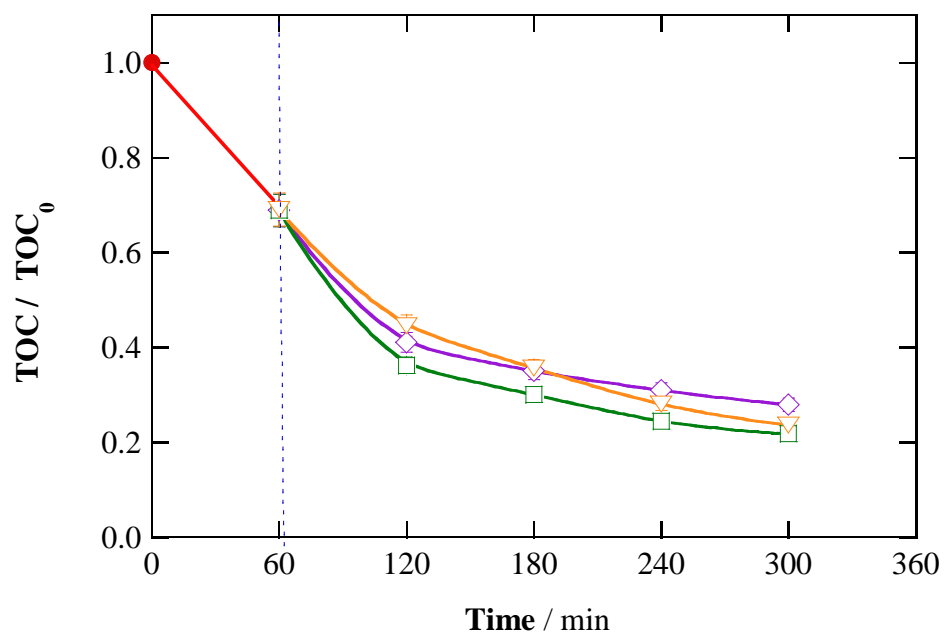


Fig. 5



**Fig. 6**



**Fig. 7**

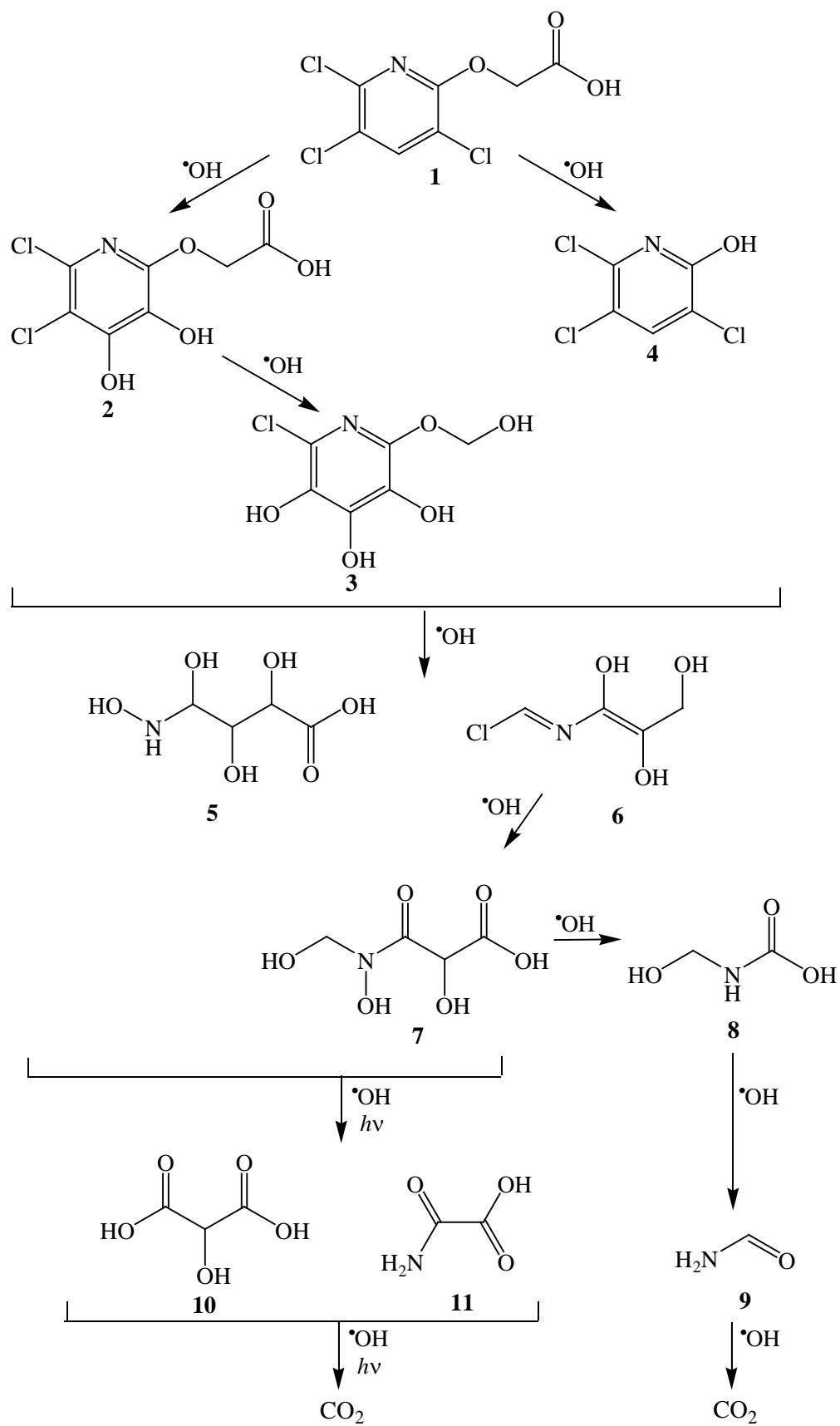


**Fig. 8**

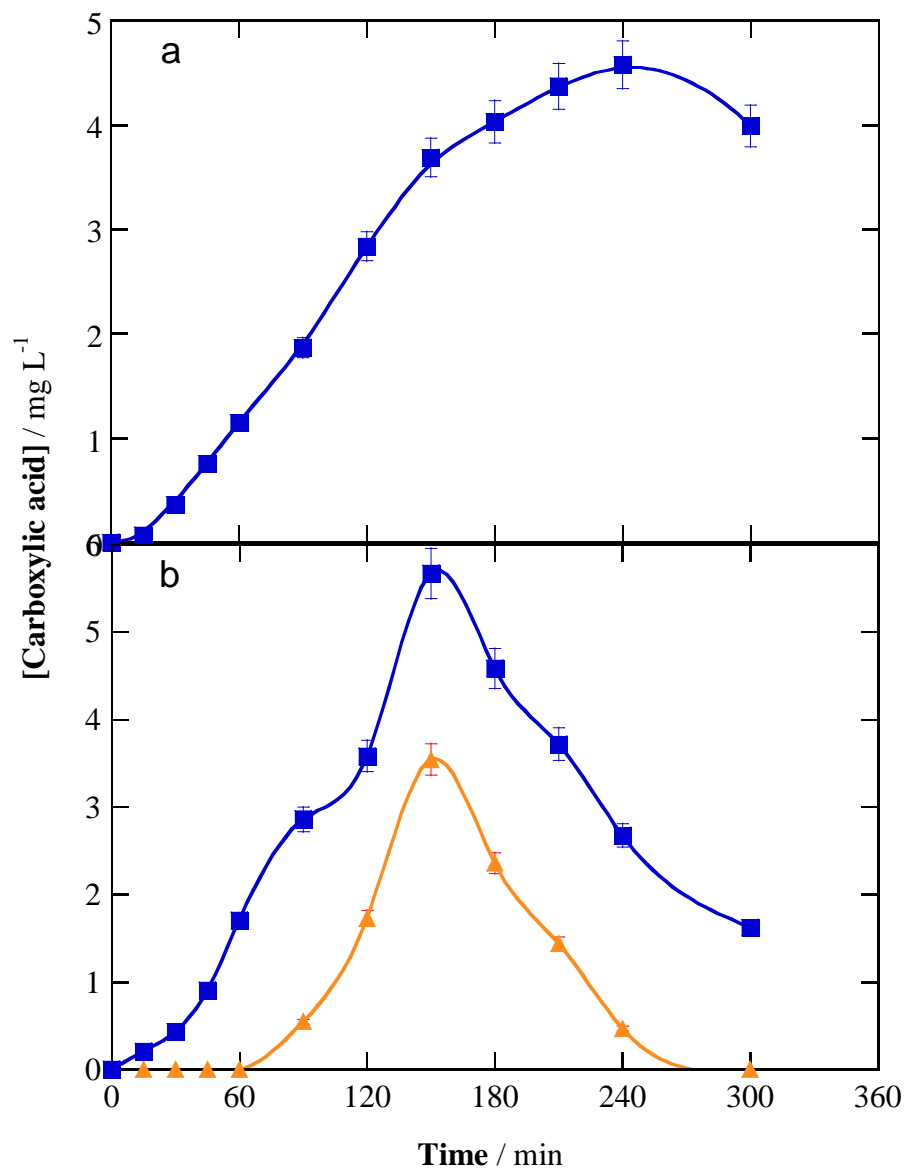


**Fig. 9**

**Table 1** Conditions and results for the treatment of 150 mL of solutions containing 0.12 mM triclopyr in 0.050 M Na<sub>2</sub>SO<sub>4</sub> with varying Fe(III)–EDDS concentration at pH 7.0 and 35 °C by EAOPs using an undivided cell with a 3 cm<sup>2</sup> anode and 3 cm<sup>2</sup> air-diffusion cathode.

Method	Anode	[Fe(III)–EDDS] <sub>0</sub> (mM)	<i>j</i> <sup>a</sup> in mA cm <sup>-2</sup> ( <i>t</i> in min)	Time for complex <sup>b</sup> (min)	<i>k<sub>c</sub></i> <sup>c</sup> (10 <sup>-2</sup> min <sup>-1</sup> )	% Triclopyr ( <i>t</i> in min)	<i>k<sub>1</sub></i> <sup>d</sup> (10 <sup>-2</sup> min <sup>-1</sup> )	% TOC removal at 300 min	EC <sub>TOC</sub> (kWh (g TOC) <sup>-1</sup> )
EO-H <sub>2</sub> O <sub>2</sub> <sup>e</sup>	IrO <sub>2</sub> -based	0.06	16.7	-	-	0	-	3.0	-
	BDD	0.06	16.7	-	-	68 (300)	0.38	38	2.34
EF	IrO <sub>2</sub> -based	0.06	16.7	> 300	0.49	30 (300)	0.17	13	3.28
	BDD	0.06	16.7	240	1.3	100 (270)	1.2	47	1.81
PEF	IrO <sub>2</sub> -based	0.06	16.7	80	4.7	100 (270)	1.2	44	0.88 (27.3) <sup>h</sup>
		BDD	0.03	16.7	80	4.8	100 (180)	2.1	66
		0.06	16.7	80	4.5	100 (180)	2.2	65	1.31 (19.2) <sup>h</sup>
		0.06	16.7 (60)+ 33.3 (240)	-	-	100 (140)	-	69	4.96 (21.8) <sup>h</sup>
		0.06	16.7 (60)+ 66.7 (240)	-	-	100 (120)	-	75	10.02 (25.5) <sup>h</sup>
SPEF	IrO <sub>2</sub> -based	0.09	16.7	80	4.8	100 (180)	2.4	62	1.19 (16.7) <sup>h</sup>
		0.06	16.7	- <sup>f</sup>	- <sup>f</sup>	100 (210)	- <sup>g</sup>	44	0.88
		0.06	16.7	- <sup>f</sup>	- <sup>f</sup>	100 (80)	5.9	62	1.33
		0.06	16.7 (60)+ 33.3 (240)	-	-	-	-	72	4.01
		0.06	16.7 (60)+ 66.7 (240)	-	-	-	-	78	9.07

<sup>a</sup> Current density; <sup>b</sup> Time for total disappearance of the complex; <sup>c</sup> *k<sub>c</sub>*: apparent rate constant for the Fe(III)–EDDS complex, with *R*<sup>2</sup> > 0.99; <sup>d</sup> *k<sub>1</sub>*: apparent rate constant for triclopyr, *R*<sup>2</sup> > 0.99; <sup>e</sup> No Fe(III) in solution; <sup>f</sup> Not determined; <sup>g</sup> No evaluation of pseudo-first-order kinetics. <sup>h</sup> Specific energy consumption per unit TOC mass when the term related to the electric energy supplied to the 6 W UVA lamp (i.e., 6 *t* / *V* (ΔTOC)), was added to Eq. (10).

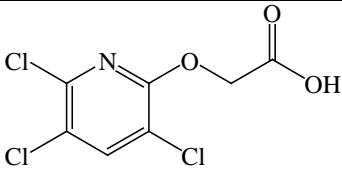
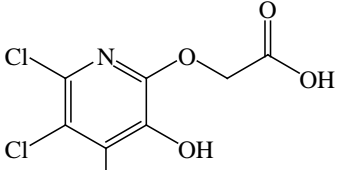
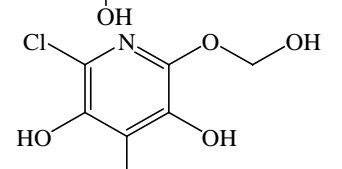
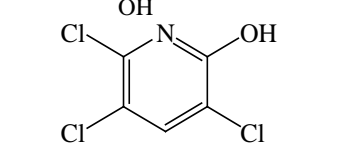
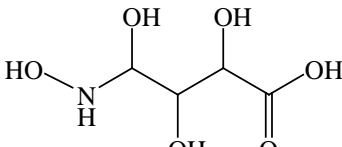
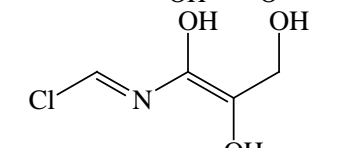
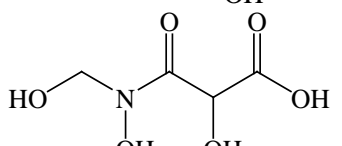
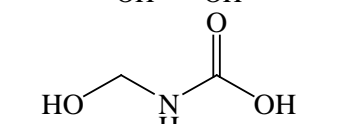
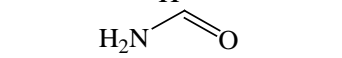


**Table 2** Conditions and results for the treatment of 150 mL of solutions containing 0.12 mM triclopyr in 0.025 M Na<sub>2</sub>SO<sub>4</sub> + 0.035 M NaCl by varying Fe(III)–EDDS concentration at pH 7.0 and 35 °C by EAOPs using an undivided cell with a 3 cm<sup>2</sup> anode and 3 cm<sup>2</sup> air-diffusion cathode.

Method	Anode	[Fe(III)–EDDS] <sub>0</sub> (mM)	<i>j</i> <sup>a</sup> in mA cm <sup>-2</sup> ( <i>t</i> in min)	Time for complex <sup>b</sup> (min)	<i>k<sub>c</sub></i> <sup>c</sup> (10 <sup>-2</sup> min <sup>-1</sup> )	% Triclopyr ( <i>t</i> in min)	<i>k<sub>1</sub></i> <sup>d</sup> (10 <sup>-2</sup> min <sup>-1</sup> )	% TOC removal at 300 min	EC <sub>TOC</sub> (kWh (g TOC) <sup>-1</sup> )
PEF	RuO <sub>2</sub> -based	0.06	25	120	8.0	100 (90)	2.1	70	0.91 (17.5) <sup>e</sup>
	IrO <sub>2</sub> -based	0.06	25	120	7.9	100 (90)	1.7	65	0.89 (18.8) <sup>e</sup>
	BDD	0.06	25	120	9.8	100 (90)	2.5	73	1.75 (17.7) <sup>e</sup>
SPEF	BDD	0.06	16.7 (60)+ 66.7 (240)	-	-	-	-	76	9.58

<sup>a</sup> Current density; <sup>b</sup> Time for total disappearance of the complex; <sup>c</sup> *k<sub>c</sub>*: apparent rate constant for the Fe(III)–EDDS complex, with  $R^2 > 0.99$ ; <sup>d</sup> *k<sub>1</sub>*: apparent rate constant for triclopyr,  $R^2 > 0.99$ ; <sup>e</sup> Specific energy consumption per unit TOC mass when the term related to the electric energy supplied to the 6 W UVA lamp (i.e.,  $6 t / V(\Delta\text{TOC})$ ), was added to Eq. (10).

**Table 3** Products identified by GC-MS after 40 min of PEF treatment of 150 mL of solutions with 0.12 mM triclopyr, 0.050 M Na<sub>2</sub>SO<sub>4</sub> and 0.06 mM Fe(III)–EDDS at pH 7.0 and 35 °C, using a BDD/air-diffusion cell at 16.7 mA cm<sup>-2</sup> under illumination with a 6 W UVA lamp.

No.	Chemical name	Molecular structure	Column <sup>a</sup>	<i>t<sub>r</sub></i> <sup>b</sup> (min)	<i>m/z</i> <sup>c</sup>	Fragments (leaving groups)
1	Triclopyr		N	32.56	255	210 (-COOH)
			P	58.59	197 (-CH <sub>2</sub> -COOH) 180 (-O-CH <sub>2</sub> -COOH) 146 (182,-Cl) 110 (146,-Cl)	
2	(5,6-Dichloro-3,4-dihydroxypyridin-2-yloxy)-acetic acid		P	54.97	254	219 (-Cl) 209 (-COOH) 179 (-O-CH <sub>2</sub> -COOH) 143 (181, -Cl)
3	2-Chloro-6-hydroxymethoxy-pyridine-3,4,5-triol		P	23.74	207	171 (-Cl)
4	3,5,6-Trichloro-2-pyridinol		N	24.27	197	169 (-CO)
			P	42.56	133 (-CO, -Cl) 107 (-COH, -C(Cl), -CH) 98 (-CO, -2Cl)	
5	2,3,4-Trihydroxy-4-hydroxyaminobutyric acid		N	44.87	167	149 (-OH, -H)
6	<i>N</i> -Chloromethylene-2,3-dihydroxypropenimidic acid		P	22.69	151	133 (-OH,-H)
7	2, <i>N</i> -Dihydroxy- <i>N</i> -hydroxymethyl-malonamic acid		P	13.52	165	135 (-CH <sub>2</sub> OH) 119 (-COOH, -H) 75 (-CO-N(OH)-CH <sub>2</sub> OH) 61 (-CO-CHOH-COOH, -H)
8	Hydroxymethyl-carbamic acid		P	10.31	91	61 (-CH <sub>2</sub> OH) 45 (-COOH, -H)
9	Formamide		P	11.65	45	30 (-NH <sub>2</sub> , +H)

<sup>a</sup> N: Non-polar, P: Polar; <sup>b</sup> Retention time; <sup>c</sup> Chloro-derivatives determined considering <sup>35</sup>Cl and <sup>37</sup>Cl.